POLITECNICO DI TORINO

Master Degree course in Mechanical Engineering

Master Degree Thesis

Analytical modelling and experimental analysis of functionalized nonlinear link for jointed structures

Supervisors

Prof. Alessandro Fasana

Prof. Nicolas Peyret

Candidate

Giuseppe Lo Iacono

Academic Year 2021-2022

Contents

List of Figures

Preface

> “Il divertimento della ricerca scientifica è anche trovare sempre altre frontiere da superare, costruire mezzi più potenti d’indagine, teorie più complesse, cercare sempre di progredire pur sapendo che probabilmente ci si avvicinerà sempre di più a comprendere la realtà, senza arrivare mai a capirla completamente.”
>
> MARGHERITA HACK

La scelta di portare avanti questo progetto di ricerca fonda le radici nella mia volontà di dare un contributo alla comunità scientifica mettendo in gioco le conoscenze acquisite durante il percorso di studi.

Dedicherò ampio spazio alla descrizione dei temi trattati, perciò approfitto di questo breve paragrafo per ringraziare tutte le persone che mi hanno sempre sostenuto consentendomi di raggiungere questo traguardo a testa alta, **perché ognuno di voi ha contribuito ad essere la persona che sono oggi**.

Mi ritengo fortunato perchè so di avere al mio fianco molte persone che ripongono in me grande affetto e stima, ma non amo gli encomi, e dunque, fra tutti, ritengo doveroso citare i miei genitori per la fiducia e il sostegno riposto in me sin dal principio, ancor prima di intraprendere il mio percorso universitario, lasciandomi libero nelle scelte e facendomi sentire sempre sicuro di me stesso.

Grazie a tutti voi.

Introduction

The aim of this study is to investigate the possibility of increasing the damping of a structure composed of two elements connected by threaded joints, by interposing mechanical dampers at the interface of the contact surface.

Indeed, one of the technological design problems engineers are faced with is undoubtedly the need to connect two or more elements together.

To this aim, engineers can rely essentially on three main mechanical joining processes: **welding, gluing and mechanical fixing**.

Mechanical fixing (screws, bolts, rivets, etc.), in particular, differs from the other two solutions because it is necessary to drill holes in the components before the joining process.

This operation inevitably causes a weakening of the component, since in the area close to the hole there is a concentration of stresses due to the high notching effect. For this reason, if the use of screws or bolts is not strictly necessary, the mechanical components are joined mainly by welding (joints obtained by gluing are not used when the applied loads increase considerably).

Thanks to scientific research, however, it has been realised that mechanical joints can be used to increase the damping capacity of structures, especially in working conditions characterised by large frequency ranges and high temperatures.

So why use mechanical joints to increase the damping of structures?

Damping induced by elastic and viscous materials is more effective than dry frictional damping, but it should be noted that this statement is consistent if you are in the right frequency and temperature range for which the coupling was designed, since the heat transferred to the coupling midifies the viscoelastic properties of the coupling, causing it to be useless for the task for which it was designed.

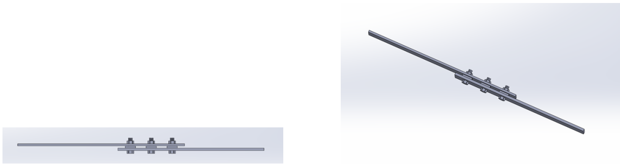

Figure 1: Assembled beam

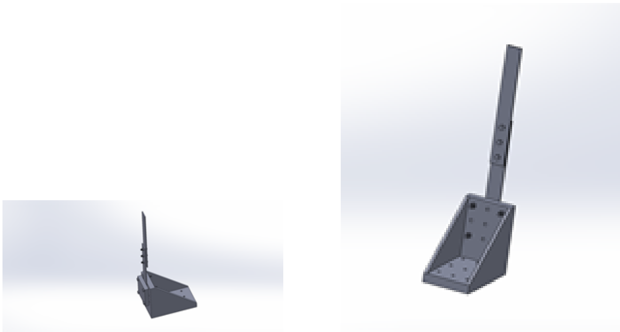

Figure 2: Coupling between base and beam

Having clarified the reasons that drive research in this area, it is possible to define the two main types of **mechanical joints**:

- **Structural joints** (Main joints), which have the task of connecting components in a purely structural sense;
- **Dissipative joints** (Secondary joints), which, in addition to physically connecting components, have the task of increasing the damping of the structure by improving its ability to absorb vibrations.

The objective of the study is firstly to compare the resonance frequency values obtained through numerical FEM simulation with the results obtained through laboratory experiments, than to estimate the damping factor of different beam configurations (beam in Figure 1) obtained by modifying the type and position of the dampers, and finally to understand which configuration provides the greatest increase in the damping factor.

About the organisation of the text, it has been divided into three macro sections:

- **First Section**: Within the first section, the main technological problems to be faced when dealing with a threaded joint are discussed. Furthermore, since the aim of the study is to evaluate the variation of the damping of the structure due to frictional dissipation, the main information concerning the mathematical models used when modelling contact in the presence of relative motion between two bodies has been summarised;

- **Second Section**:The second section is firstly dedicated to the description of the experimental tests carried out in the laboratory, and to the comparison between the simulation results carried out on Ansys and the experimental ones regarding the first four resonance frequencies of the system. Finally, this section is dedicated to the discussion of the results obtained with the different configurations of dampers inserted in the beam.
- **Third Section** : The third section corresponds to the last chapter, which is dedicated to conclusions is devoted to conclusions.

Chapter 1

State of art

1.1 Threaded links

When it is necessary to join two or more components, it is possible to use, among other methods, screws or bolts.

This type of joint modifies the stiffness of the structure as the tightening torque varies and, therefore, if the structure is very stiff, it becomes more sensitive to resonance. In order to attenuate this phenomenon by improving the damping effect of the structure, it is possible to modify the working conditions of the joint at the interface between the contact surfaces of the components by interposing an elastic metal material that acts as a damper and does not further stiffs the structure.

Before going into the mathematical modeling of the problem, could be useful remembering how a mechanical joint works.

As can be seen in Figure 1.1, different pressure distributions may occur by varying the tightening torque or the thickness of the plates. These differences in the pressure distribution result in a different stiffness of the joint and consequently in the total stiffness of the structure, in fact, generally, it is possible to consider the joints as a series of springs in compression:

$$\frac{1}{K} = \sum_i \frac{1}{k_i} \tag{1.1}$$

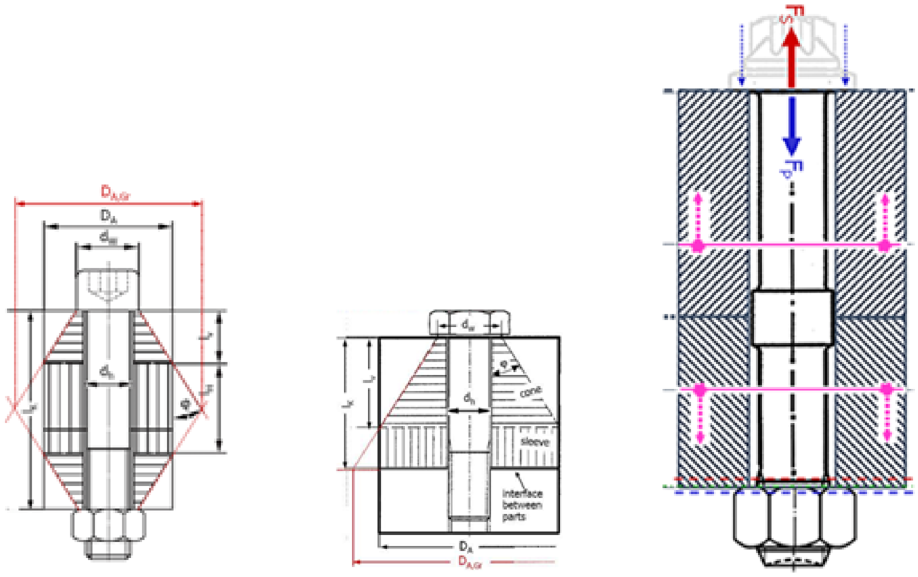

Figure 1.1: Pressure distribution in a threaded joint [Eugenio Brusa, Machine design, DIMEAS, Politecnico di Torino, Italia, 2020]

$$k_i = \frac{\pi E d \tan\phi}{2\ln\frac{(l\tan\phi + d_w - d)(d_w + d)}{(l\tan\phi + d_w + d)(d_w - d)}} \tag{1.2}$$

It is therefore easy to understand that as the contact area between the two surfaces varies, so does the static and dynamic behaviour of the joint.

1.2 Choice of beam geometry

In order to assess the stiffness of the joint, several fixing solutions were considered.

Of the different solutions proposed, the solution in Figure 1.2c was chosen, as this configuration does not significantly increase the stiffness of the structure but at the same time allows the dampers to work with a large contact surface.

What is expected from the experimental evidence is a decrease in the amplitude of the resonance peak as shown in Figure 1.4 due to the friction between the dampers and the beam.

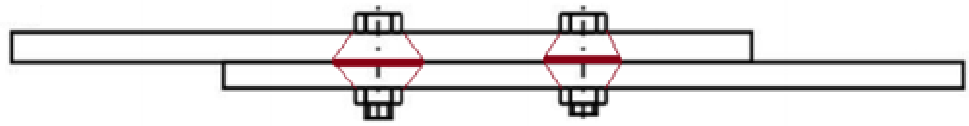

(a) *Full contact i the interface*

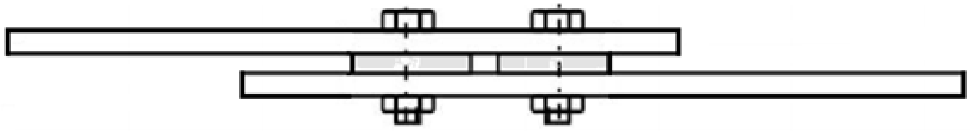

(b) *Insertion of patch*

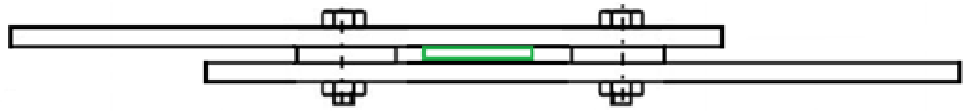

(c) *Insertion flexible friction damper, green element*

Figure 1.2: Configuration of the joint interface surfaces

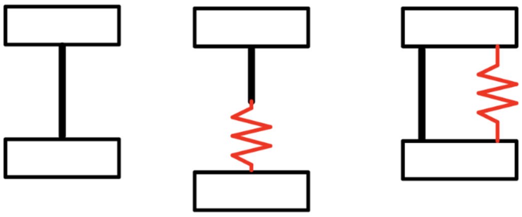

(a)

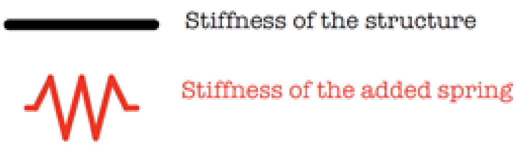

(b)

Figure 1.3: Rheological scheme of configurations a) b) c)

1.3 Mathematical models for contact modelling

In the system analysed (two beams joined by using of three bolts) the main causes of energy dissipation and consequently of the increase in damping of the structure are essentially two, namely the **deformation of the dampers** and the **friction** generated at the interface between the dampers and the two beams.

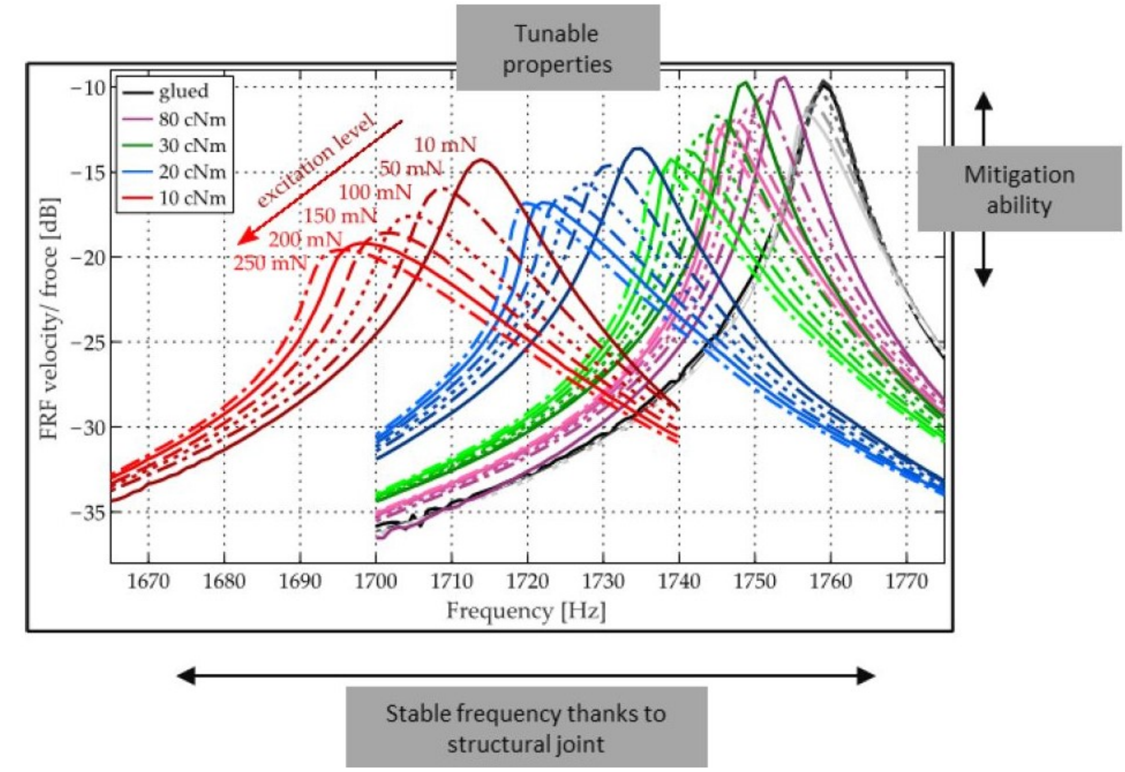

Figure 1.4: FRF variation as a function of tightening and exitation level [5]

Given the presence of the two jointed elements, it is evident that in correspondence of the interface between the two beams and the interface between the beam and the dampers, dynamic friction is generated due to the relative displacement between the bodies.

Effectively, what happens during the excitation of the system is a variation of the oscillation phase angle between the lower portion of the beam, which is wedged, and the upper portion, which is bound to it; this is due to the presence of the joint, which is a discontinuity zone between the two bodies.

The consequence of this displacement is the relative motion between the two bodies and consequently the presence of the friction force that absorbs energy from the system.

This phenomenon is called "stick-slip" (the name derives the relative motion and by the modulus of the velocity, which alternatively is equal to zero).

To study the stick-slip phenomenon, the scientific literature proposes a number of mathematical models that can be classified into two macro groups:

- Micro sliding friction models

- Macro models.

The modelling of friction for the prediction and control of such a system is quite complicated. The difficulty arises from the fact that the direction of movement on the two contact surfaces can change the friction effect. There are numerous friction models studied in the context of micro and macro-motion, such as the Coulomb friction model, viscous friction model, Stribeck friction model, Dahl model, LuGre model and the elastoplastic friction model, but despite this, the complexity of the phenomenon makes it difficult to correctly interpret the results obtained through these models.

1.4 Micro sliding friction model

This class of models is based on the distribution of shear and normal stresses according to the contact plane and the contribution of tangential displacement in order to describe the effect of contact. The literature suggests that the main improvements to this type of model can be several, the main ones being the creation of a tensile stress at the rear of the contact zone, related to the direction of movement assuming that the maximum shear point moves forward into the new contact zone; at the front of the contact zone, on the other hand, the addition of a compressive constraint much larger than the calculated maximum Hertz pressure is considered. Tangential reciprocating loading causes wear and fatigue in the contact zone, so it is essential to recognise the slip zone and the stick zone.

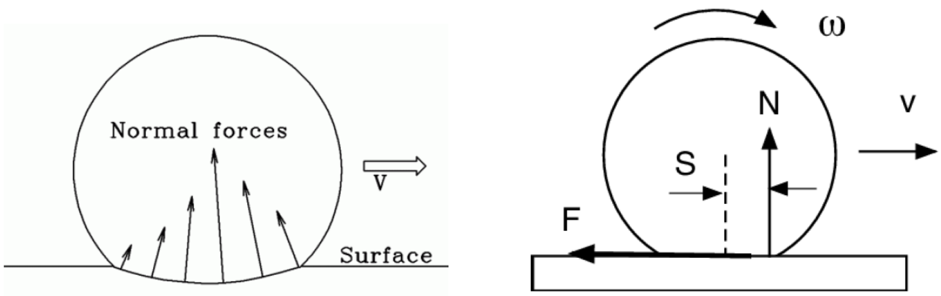

Figure 1.5: Micro sliding friction model [3]

1.5 Macro models

The set of the main macro-models can be divided into the following sub-groups:

- **Quasi-static friction models**: they are generally considered as classical friction models, since the main assumption is that the friction force depends on the relative velocity between the two bodies in the contact zone;
- **Dynamic models**: In order to model the force-slip dependence, the shape function of the stress-strain curve is used (this is the theory on which Dahl's model is based);
- **Hysteretic models**: related to the dissipation of energy in the material and the theory of elasticity.

1.5.1 Coulomb (Quasi-static friction model)

The Coulomb model can be summarised using the following system of equations:

$$F = \begin{cases} F_c \cdot \text{sgn}(\dot{x}) & \text{if} \quad \dot{x} \neq 0 \\ F_{app} & \text{if} \quad \dot{x} = 0 \quad \textit{and} \quad F_{app} < F_c \end{cases}$$

where:

- $\mathbf{F}$ is the friction force
- $\dot{\mathbf{x}}$ is sliding velocity
- $\mathbf{F_{app}}$ is applied force
- $\mathbf{F_c}$ is the Coulomb friction force, defined as $F_c = \mu F_N$
- $\boldsymbol{\mu}$ is the Coulomb friction coefficient (or dynamic friction coefficient)
- $\mathbf{F_N}$ is the normal load acting between the two surfaces in contact

A graphical representation of the Coulomb model is presented in Figure 1.6.

As can be seen in the plot, when $F_{app} < F_c$, there is no sliding between two contact surfaces, and therefore the static friction force can assume any value as long as it is between 0 and F_c.

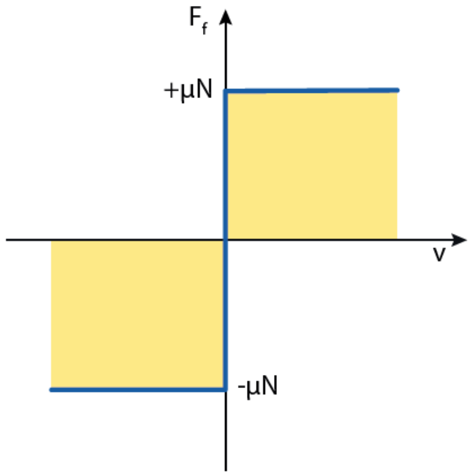

Figure 1.6: Coulomb model scheme [5]

If $\dot{x} \neq 0$, the Coulomb friction force assumes only F_c or $-F_c$ values, depending on the direction of sliding.

Being rather simple, the Coulomb friction model can be used in applications such as the prediction of temperature distribution in bearings design and the calculation of shear force in machine tools.

However, due to fact that in absence of relative displacement between the two courses the static friction force remains undefined, it is generally not used in applications where the "Stick-slip" phenomenon is persistent.

1.5.2 Viscous friction model (Quasi-static friction model)

The viscous friction model is given by:

$$F = k_v \dot{x}, \tag{1.3}$$

Where:

- **F** is the friction force;
- $\mathbf{k_v}$ the viscous coefficient;
- $\dot{\mathbf{x}}$ the sliding velocity.

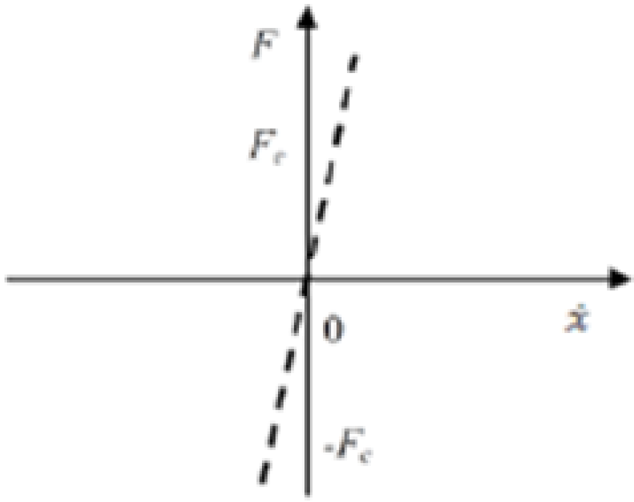

Figure 1.7: Viscous model scheme

The viscous friction model is illustrated in Figure 1.7 and, as is possible to detect from the plot, the friction force is a linear equation of the sliding velocity.

1.5.3 Integrated Coulomb and friction model (Quasi-static friction model)

The Coulomb and viscous friction models can be combined in two different ways.

The first method involves modelling the phenomenon using the following system of equations:

$$F = \begin{cases} F_c \cdot \mathrm{sgn}(\dot{x}) + k_v \dot{x} & \text{if} \quad \dot{x} \neq 0 \\ F_{app} \quad \text{if} \quad \dot{x} = 0 \quad and \quad F_{app} < F_c \end{cases}$$

The problem with this model, Figure 1.8a, is that the frictional force remains "undefined" when the relative velocity is zero. To overcome this problem, the idea is to integrate the Coulomb model and the viscous model near $\dot{x} = 0$.

$$F = \begin{cases} min(F_c, k_v \dot{x}) & \text{if} \quad \dot{x} \geq 0 \\ max(-F_c, k_v \dot{x}) & \text{if} \quad \dot{x} < 0 \end{cases}$$

Through this model, the speed of the friction force transition (from negative to positive) is determined by the viscous friction coefficient (Figure 1.8b).

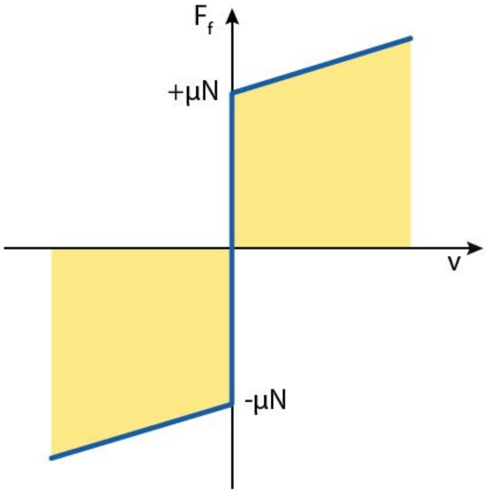

(a)

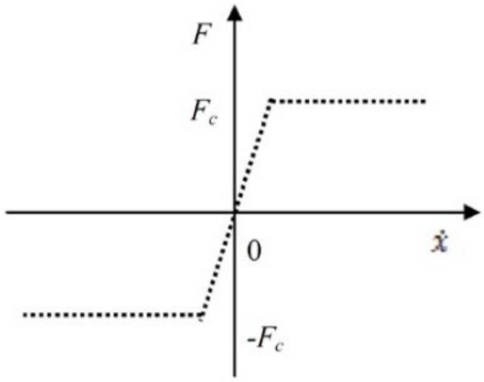

(b)

Figure 1.8: Integrated Coulomb and viscous model [5]

1.5.4 Stribeck friction model (Quasi-static friction model)

The Stribeck model is described by:

$$\left(F_c + (F_s - F_c)(e^{-\frac{\dot{x}}{v_s}})^i \cdot \mathrm{sgn}(\dot{x}) + k_v \dot{x}\right) \tag{1.4}$$

where:

- **F** is the friction force;
- $\dot{\mathbf{x}}$ is the sliding velocity;
- $F_{\mathbf{c}} = \mu N$ the Coulomb friction force;
- $\mathbf{F_s}$ the static friction force;
- $\mathbf{v_s}$ the Stribeck velocity;
- $\mathbf{k_v}$ the coefficient of viscous friction;
- **i** an parameter.

The singular feature of this model,Figure 1.9, is that when the velocity is zero, the force can range from F_s as the upper limit and $-F_s$ as the lower limit. Thanks to this

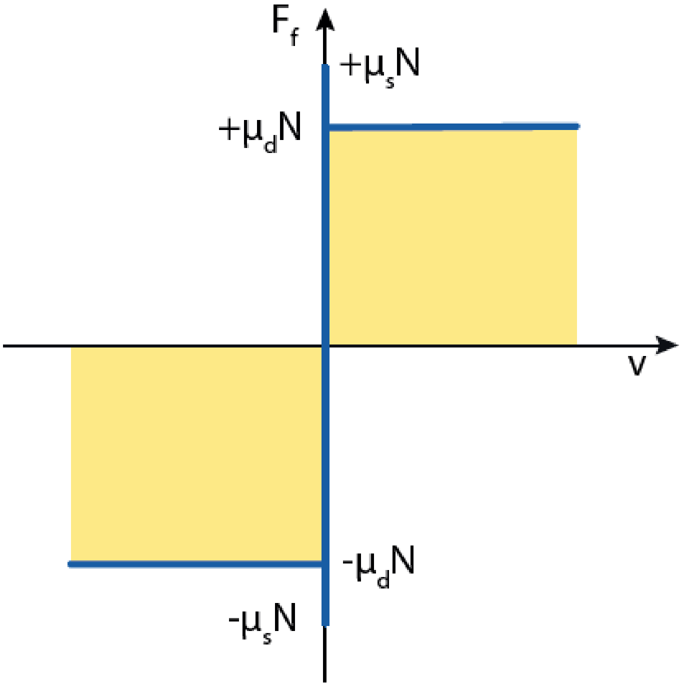

Figure 1.9: Stribeck model [5]

model it is possible to appreciate a decrease of the friction force when the movement starts and then an increase when the speed increases.

1.5.5 Dahl friction model (Dynamic model)

Dahl's model is of great interest because thanks to his theory it is possible to describe the friction force in the pre-slip phase, which remained unknown in Stribeck's model. This is one of the models that will be used to estimate the damping factor.

The two main equations which describe the model are:

$$\begin{cases} \dfrac{dF(x)}{dt} = \dfrac{dF(x)}{dx}\dfrac{dx}{dt} \\ \dfrac{dF(x)}{dx} = \sigma_0 \left|1 - \dfrac{F}{F_c}\mathrm{sgn}(\dot{x})\right|^i \mathrm{sgn}(1 - \dfrac{F}{F_c}\mathrm{sgn}(\dot{x})) \end{cases}$$

Where:

- **F** is the friction force

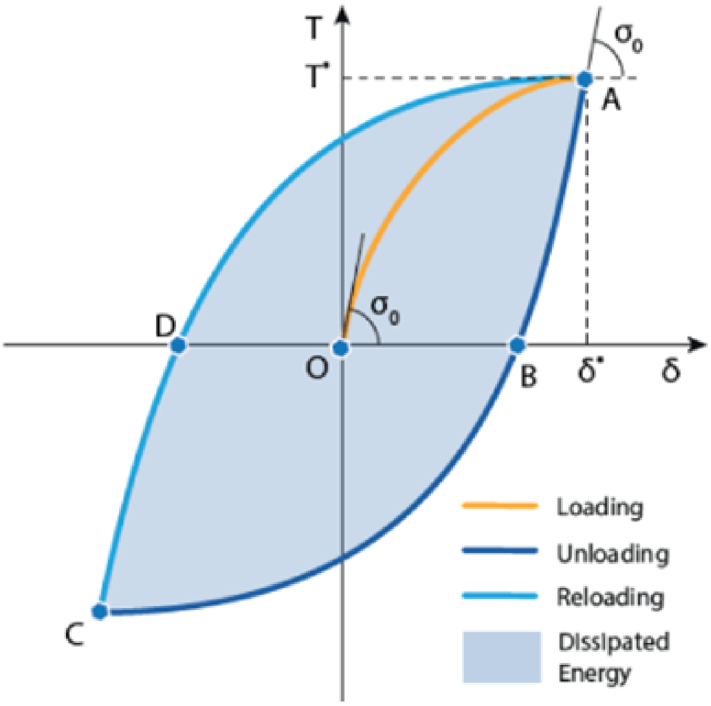

Figure 1.10: Dahl generic cycle [5]

- σ_0 the stiffness coefficient
- **i** is the exponent determining the shape of the hysteresis.

In the literature, Dahl's model is often simplified with the exponent i=1 and given by:

$$\frac{dF(x)}{dx} = \sigma_0 \left(1 - \frac{F}{F_c}\text{sgn}(\dot{x})\right) \tag{1.5}$$

The generic shape of Dah'l hysteresis loop is s shown in Figure 1.10, but as the parameters of the system vary, it can vary considerably. Some examples of the hysteresis loop are shown in Figure 1.11.

However, as the parameters of the equation describing the model change, the curve can assume different shapes

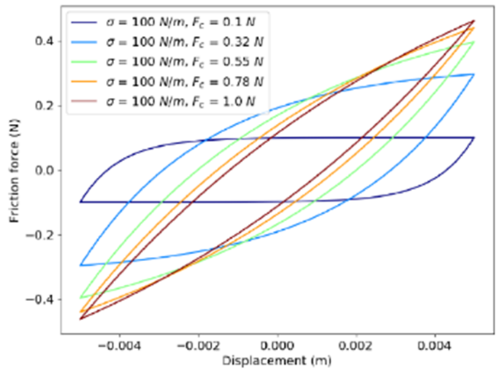

(a) Variation of contact force "F_c"

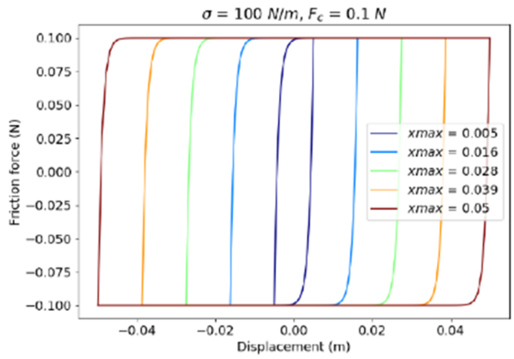

(b) Variation of maximum desplacement

Figure 1.11: Shape of Dahl hysteresis cycle as function of different parameters [5]

1.5.6 LuGre friction model (Dynamic model)

Lugre's model can be expressed as follows:

$$\begin{cases} F = \sigma_0 z + \sigma_1 \dot{z} + \sigma_2 \dot{x} \\ \dot{z} = \dot{x} - \sigma_0 \dfrac{\dot{x}}{g(\dot{x})} z \\ g(\dot{x}) = F_c + (F_s - F_c)(e^{-\frac{\dot{x}}{v_s}})^j \end{cases}$$

where:

- **F** is the frictional force
- σ_0 the contact stiffness
- **z** the mean deflection of contact asperities

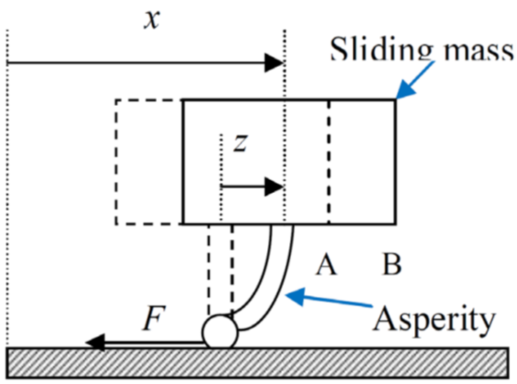

Figure 1.12: Deformation of the asperity in the interface [4]

- σ_1 the bristle damping coefficient
- σ_2 the coefficient of viscous friction
- $\mathbf{x}$ the relative displacement
- $\mathbf{F_c}$ the Coulomb friction force F_s the static friction force
- $\dot{\mathbf{x}}$ the sliding velocity
- $\mathbf{g(\dot{x})}$the Stribeck effect
- $\mathbf{v_s}$ the Stribeck velocity
- $\mathbf{j}$ the Stribeck form factor

The LuGre model integrates pre-slip friction $\sigma_0 z$, viscous friction $\sigma_2 \dot{x}$ and the Stribeck effect $g(\dot{x})$ into a single model and is therefore used in the modelling of mechanical couplings.

Chapter 2

Experimental protocol

2.1 Introduction

The aim of the experimental tests is to obtain the frequency responce function and the acceleration signal in time domain of the beam wedged in an oscillating base.

At the interface between the two parts of the beam some dampers will be inserted in order to modify the frequency response of the system by changing the damping effect of the structure.

2.2 Tools preparation

This section details all the steps required to prepare the equipment:

- The shaker Figure 2.1 shall be positioned horizontally so that the vibrating table Figure 2.2 can vibrate in a direction parallel to the floor Figure 2.3;
- The base Figure 2.4 must be fixed to the vibrating table by means of four M10 threaded screws in the position described in Figure 2.5;
- The fastening block Figure 2.6 must be positioned, and not yet completely fixed waiting for the beam to be inserted, in the position described in Figure 2.7 (!! Pay attention to the orientation of the component Figure 2.7 !!) by means of 4 bolts M10;

Figure 2.1: Shaker

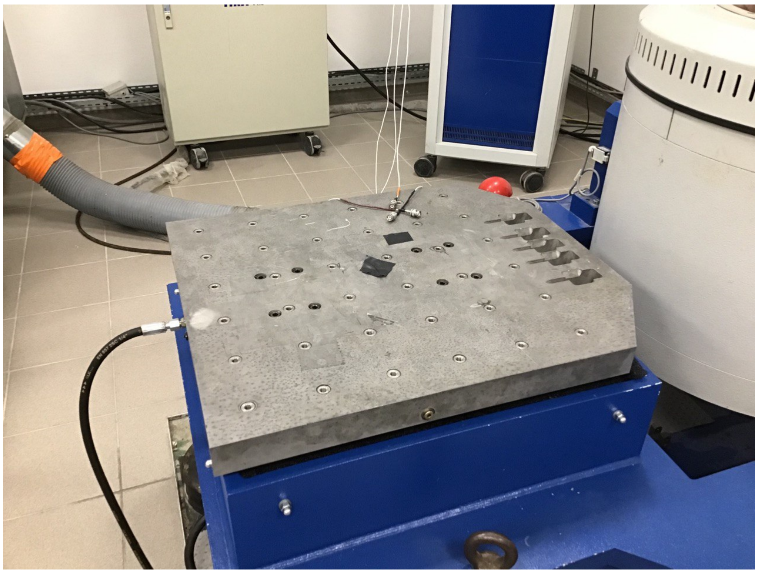

Figure 2.2: Vibrating table

- The two accelerometers must be connected to the instrumentation and ready to be connected to the two beams (In Figure 2.8a and Figure 2.8d is represented the final position of the two accelerometers);

- A thermocouple Figure 2.9 is added to evaluate the temperature variation of the beam

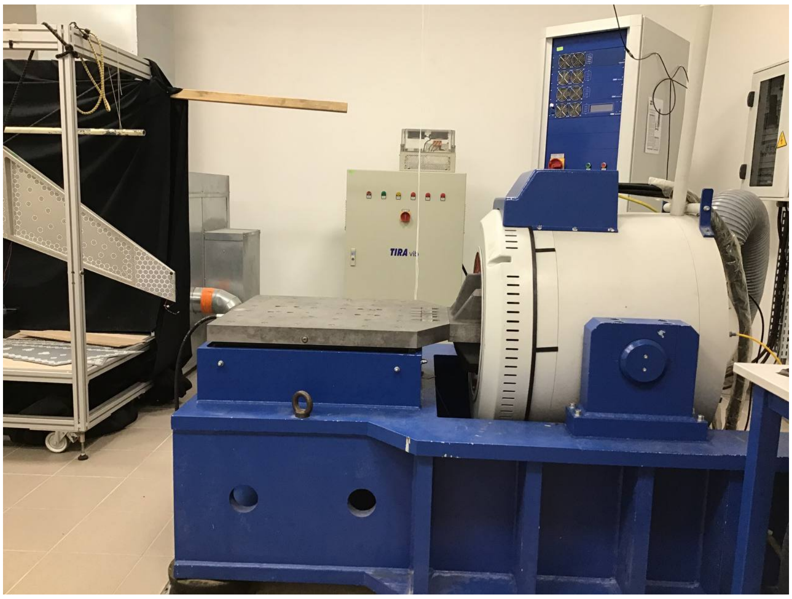

Figure 2.3: Shaker position

Figure 2.4: Figures/Base

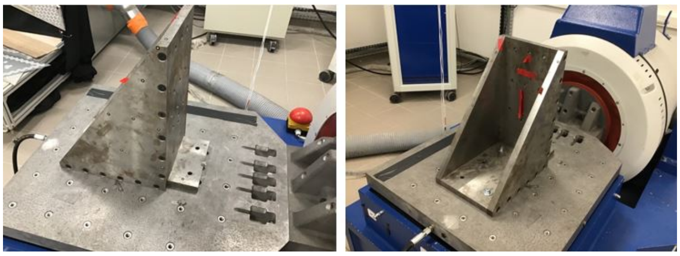

Figure 2.5: Base position

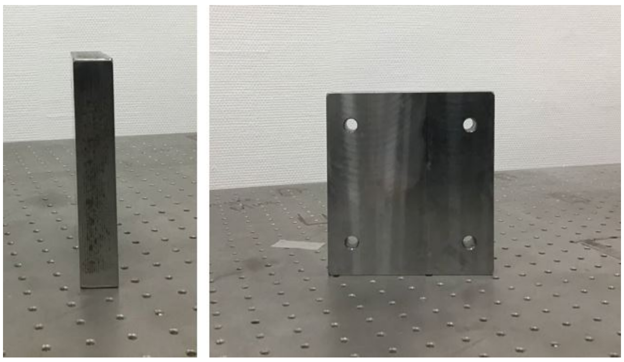

Figure 2.6: Fastening Block

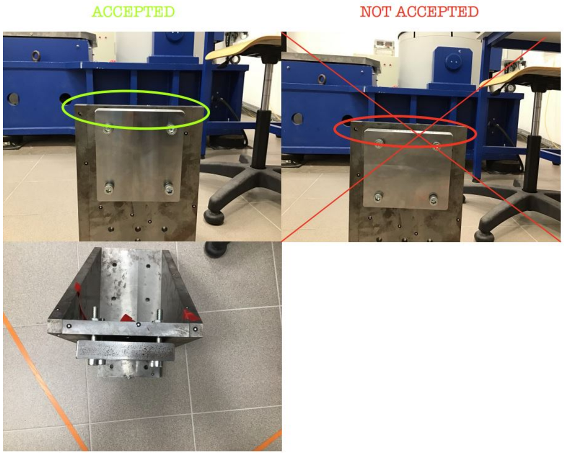

Figure 2.7: Block position

(a) Characteristics accelerometer 3

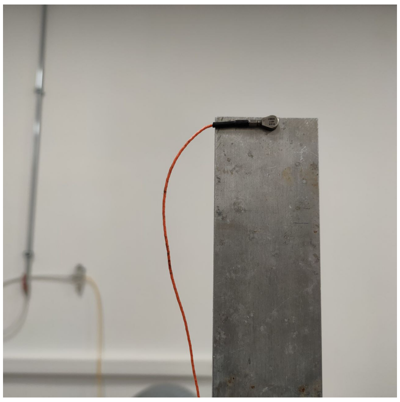

(b) Position accelerometer 3

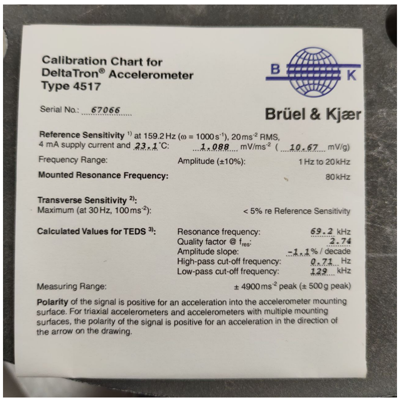

(c) Characteristics accelerometer 2

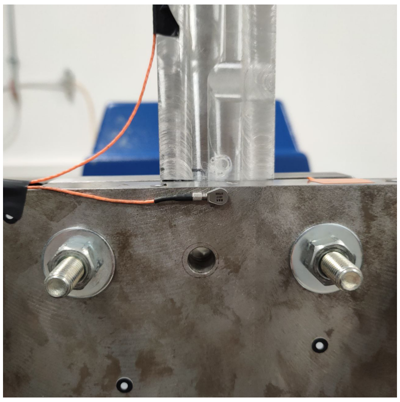

(d) Position accelerometer 2

Figure 2.8: Characteristics and Positions of the accelerometrs

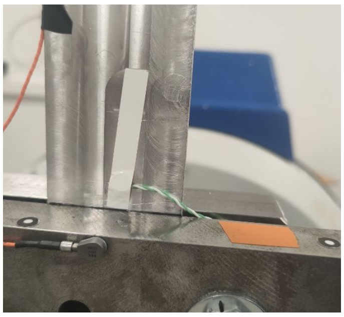

(a) Thermo-couple position

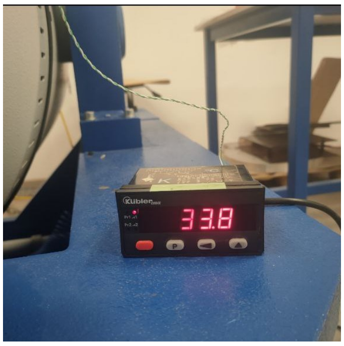

(b) Thermo-couple display

Figure 2.9: Thermo Couple

2.3 Configurations description

This section concerns the description of all the configurations used in the experiments.

Configuration 1: coupling without damper

- The uppert part of the beam in Figure 2.10 have to be fixed to the bottom part Figure 2.11 using three M10 bolts with a tightening torque of 15Nm per bolt (Figure 2.12);
- The assembled beam have to be wedged between the base and the fastening bloc using four M10 bolts, in the position shown in Figure 2.13, at a distance of 50mm from the beam's base;
- The two accelerometers must be fixed in the position described in Figure 2.8.

2.3.1 Configuration 2: coupling with Type1 damper, configuration of 2 dampers, one on each side

- The Type1 damper in Figure 2.14 have to be positioned as in Figure 2.15;
- The upper part of the beam in Figure 2.10 have to be fixed to the bottom part Figure 2.11 using three M10 bolts with a tightening torque of 15Nm per bolt (Figure 2.12);
- The assembled beam have to be wedged between the base and the fastening bloc using four M10 bolts, in the position shown in Figure 2.13, at a distance of 50mm

Figure 2.10: Top of the beam assembly

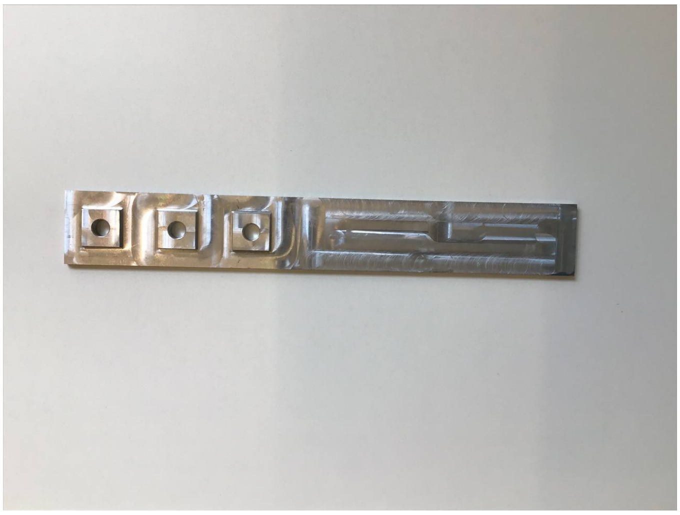

Figure 2.11: Bottom of the beam assembly

from the beam's base;

- The two accelerometers must be fixed in the position described in Figure 2.8.

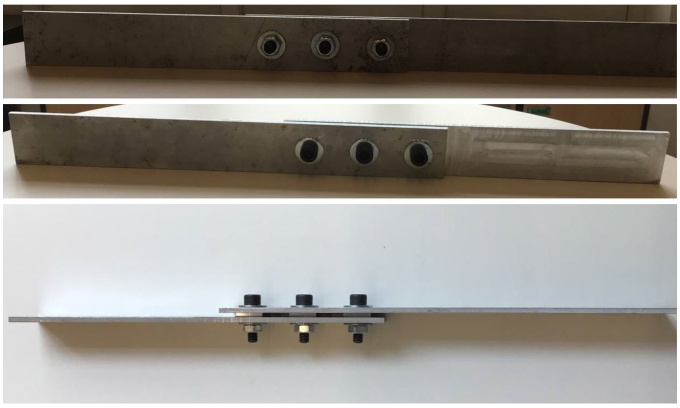

Figure 2.12: Beam assembly

Figure 2.13: Beam fastening position

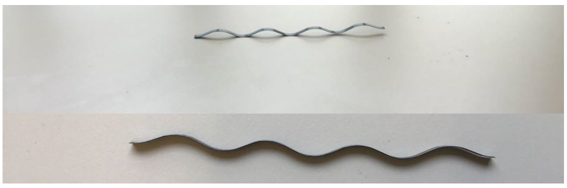

Figure 2.14: Type1 damper

2.3.2 Configuration 3: coupling with Type 1 damper, configuration of 4 dampers, two on each side, in phase

- The Type1 damper in Figure 2.14 have to be positioned as in Figure 2.16;

Figure 2.15: Damper position experiment 2

Figure 2.16: Damper position configuration 3

- The upper part of the beam in Figure 2.10 have to be fixed to the bottom part Figure 2.11 using three M10 bolts with a tightening torque of 15Nm per bolt (Figure 2.12);
- The assembled beam have to be wedged between the base and the fastening bloc using four M10 bolts, in the position shown in Figure 2.13, at a distance of 50mm from the beam's base;
- The two accelerometers must be fixed in the position described in Figure 2.8.

2.3.3 Configuration 4: coupling with Type 1 damper, configuration of 4 dampers, two on each side,in counterphase

- The Type1 damper in Figure 2.14 have to positioned as in Figure 2.17;

Figure 2.17: Damper position configuration 4

- The upper part of the beam in Figure 2.10 have to be fixed to the bottom part Figure 2.11 using three M10 bolts with a tightening torque of 15Nm per bolt (Figure 2.12);
- The assembled beam have to be wedged between the base and the fastening bloc using four M10 bolts, in the position shown in Figure 2.13, at a distance of 50mm from the beam's base;
- The two accelerometers must be fixed in the position described in Figure 2.8.

2.3.4 Configuration 5: coupling with Type 1 damper, configuration of 4 dampers, two on each side, stacked

- The Type1 damper in Figure 2.14 have to be positioned as in Figure 2.18;
- The upper part of the beam in Figure 2.10 have to be fixed to the bottom part Figure 2.11 using three M10 bolts with a tightening torque of 15Nm per bolt (Figure 2.12);
- The assembled beam have to be wedged between the base and the fastening bloc using four M10 bolts, in the position shown in Figure 2.13, at a distance of 50mm from the beam's base;
- The two accelerometers must be fixed in the position described in Figure 2.8.

Figure 2.18: Damper position experiment 5

2.3.5 Configuration 6: coupling with Type 1 damper, configuration of 6 dampers, three on each side, stacked

- The Type1 damper in Figure 2.14 have to be positioned as in Figure 2.19;
- The upper part of the beam in Figure 2.10 have to be fixed to the bottom part Figure 2.11 using three M10 bolts with a tightening torque of 15Nm per bolt (Figure 2.12);
- The assembled beam have to be wedged between the base and the fastening bloc using four M10 bolts, in the position shown in Figure 2.13, at a distance of 50mm from the beam's base;
- The two accelerometers must be fixed in the position described in Figure 2.8.

2.3.6 Configuration 7: Type2 damper coupling, 3 damper configuration

- The Type2 damper in Figure 2.20 have to be positioned as in Figure 2.21;
- The upper part of the beam in Figure 2.10 have to be fixed to the bottom part Figure 2.11 using three M10 bolts with a tightening torque of 15Nm per bolt (Figure 2.12);
- The assembled beam have to be wedged between the base and the fastening bloc using four M10 bolts, in the position shown in Figure 2.13, at a distance of 50mm from the beam's base;

Figure 2.19: Damper position experiment 6

Figure 2.20: Type2 damper

- The two accelerometers must be fixed in the position described in Figure 2.8.

2.3.7 Configuration 8: Type3 damper coupling, 3 damper configuration

- The Type2 damper in Figure 2.22 have to be positioned as in Figure 2.21;
- The upper part of the beam in Figure 2.10 have to be fixed to the bottom part Figure 2.11 using three M10 bolts with a tightening torque of 15Nm per bolt (Figure 2.12);
- The assembled beam have to be wedged between the base and the fastening bloc using four M10 bolts, in the position shown in Figure 2.13, at a distance of 50mm

Figure 2.21: Damper position experiment 7

Figure 2.22: Type3 damper

from the beam's base;

- The two accelerometers must be fixed in the position described in Figure 2.8.

2.4 List of experiments

This section will explain all the experiments carried out:

Experiment 1, Frequency scan 0-900Hz 900-0Hz 0-500Hz 500-0Hz, Configuration 1 - Configuration 2

Aim of the experiment: To obtain a precise visualisation of the beam's vibration modes.

Balayage croissate (Hz)	Balayage dècroissante (Hz)	octave/minutes	Acceleration
0-900	900-0	0,5	1g
0-500	500-0	0,5	1g

Table 2.1: Experiment 1: Experimental parameters

Experiment 2, Frequency scan 0-23Hz, Configuration 1 - Configuration 2 - Configuration 3 - Configuration 4 - Configuration 5 - Configuration 6 - Configuration 7 - Configuration 8

Aim of the experiment: Comparison of the peak of the Spectrum (where the spectrum represent the module in frequency domain of the output only) and FRF (where the FRF represent the module in frequency domain of the output/input ratio) of the damping factor for the first mode shape.

Configuration	Frequency range (Hz)	octave/minutes	Acceleration
ALL	0-23	0,5	0,8g-1,6g

Table 2.2: Experiment 2: Experimental parameters

Experiment 3, Frequency scan 55-85Hz, Configuration 1 - Configuration 2 - Configuration 3 - Configuration 4 - Configuration 5 - Configuration 6 - Configuration 7 - Configuration 8

Aim of the experiment: Comparison of the peak of the Spectrum (where the spectrum represent the module in frequency domain of the output only) and FRF (where the FRF represent the module in frequency domain of the output/input ratio) in order to evaluate the variation of the damping factor for the second mode shape.

Configuration	Frequency range (Hz)	octave/minutes	Acceleration
ALL	55-85	0,5	0,8g-1,6g

Table 2.3: Experiment 3: Experimental parameters

Experiment 4, Frequency scan 0-23Hz, Configuration 1 - Configuration 4 - Configuration 8

Aim of the experiment: Compare the peaks of the Spectrum and FRF of the best configurations related to the first mode shape. More specifically, the best results are obtained by using configuration 4 and configuration 8.

Configuration	Frequency range (Hz)	octave/minutes	Acceleration
1	0-23	0,5	0,8g-1,2g-1,6g
4	0-23	0,5	0,8g-1,2g-1,6g
8	0-23	0,5	0,8g-1,2g-1,6g

Table 2.4: Experiment 4: Experimental parameters

Experiment 5, Frequency scan 55-85Hz, Configuration 1 - Configuration 4 - Configuration 8

Aim of the experiment: Compare the peaks of the Spectrum or FRF of the best configurations related to the second mode shape). More specifically, also for the second mode shape, the best results are obtained by using configuration 4 and configuration 8.

Configuration	Frequency range (Hz)	octave/minutes	Acceleration
1	55-85	0,5	0,8g-1,2g-1,6g
4	55-85	0,5	0,8g-1,2g-1,6g
8	55-85	0,5	0,8g-1,2g-1,6g

Table 2.5: Experiment 4: Experimental parameters

Summary of experiments:

Configuration	Frequency range (Hz)	octave/minutes	Acceleration
ALL	0-23	0,5	0,8g-1,6g
ALL	55-85	0,5	0,8g-1,6g
1	0-23	0,5	0,8g-1,2g-1,6g
4	0-23	0,5	0,8g-1,2g-1,6g
8	0-23	0,5	0,8g-1,2g-1,6g
1	55-85	0,5	0,8g-1,2g-1,6g
4	55-85	0,5	0,8g-1,2g-1,6g
8	55-85	0,5	0,8g-1,2g-1,6g

Table 2.6: List of experiment

Chapter 3

FEM and Experimental Tests

3.1 Ansys and Experiments comparison (Config.1, without dampers)

This section is dedicated to the description of the results obtained through finite element method carried out on Ansys and the results obtained in the laboratory, concerning the identification of four modes shapes of the beam. The beam is made of aluminium, the bolts used are M10 and the global assembly weight is around 0.7 kg. The effect of gravity is not taken into account because the beam oscillates in a vertical position and the displacement of the centre of mass is negligible.

The images in Figure 3.1, Figure 3.2 and Figure 3.3 show the technical drawing of the beam and the real assembled beam

3.1.1 Ansys Simulation

The simulation on Ansys was carried out starting from the beam model produced by CAD on SolidWorks Figure 1. As far as the boundary conditions are concerned it should be pointed out that, as can be read in the experimental protocol, the beam is wedged between the base (Figure 2.5) and the fixing block (Figure 2.7) at a depth of 50 cm, therefore in order to realize a simulation of the wedging as similar as possible to the real condition, the constraint was applied to the two faces of the lower part of the beam starting from the lower side and up to a height of 50 cm (Figure 3.4).

At the interface between the two beam sections, since the configuration analysed is the

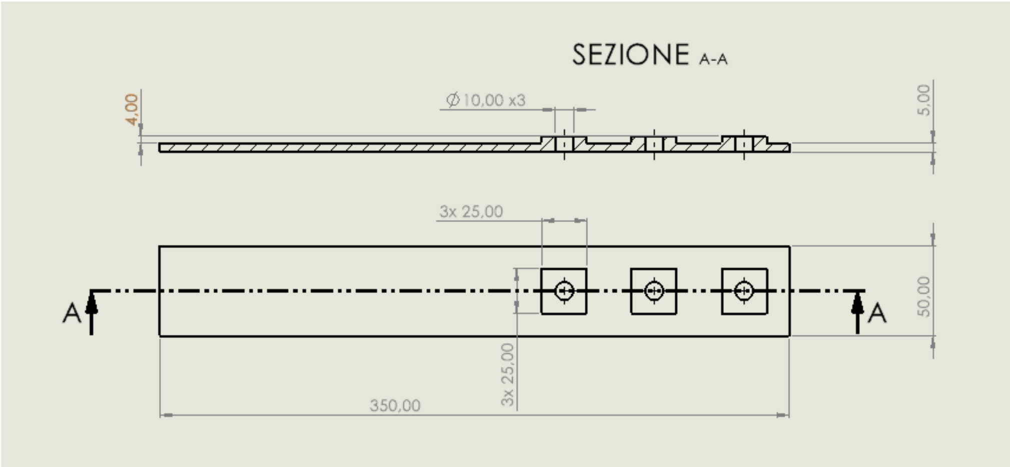

Figure 3.1: Lower part of the beam

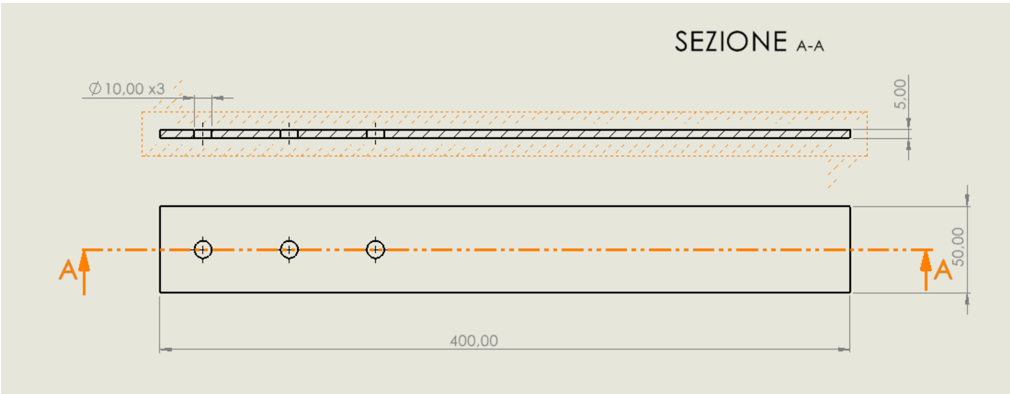

Figure 3.2: Upper part of the beam

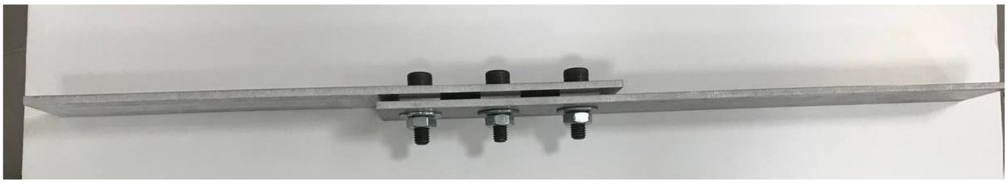

Figure 3.3: Real beam

one without dampers, an interlocking boundary condition was applied in all directions. The next step was to simulate the sinusoidal sweep, imposing a base displacement along the z-axis Figure 3.5.

Simulation Results:

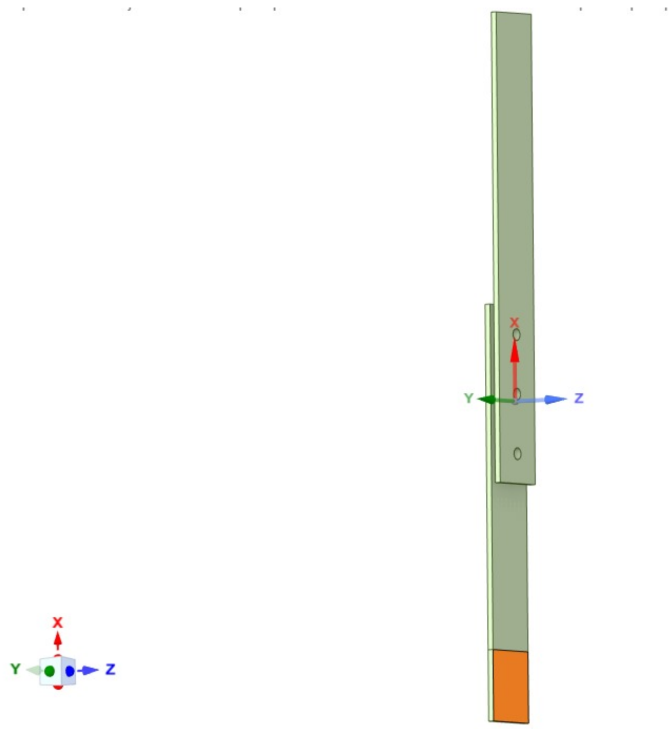

Figure 3.4: Ansys: Simulation of the constraint

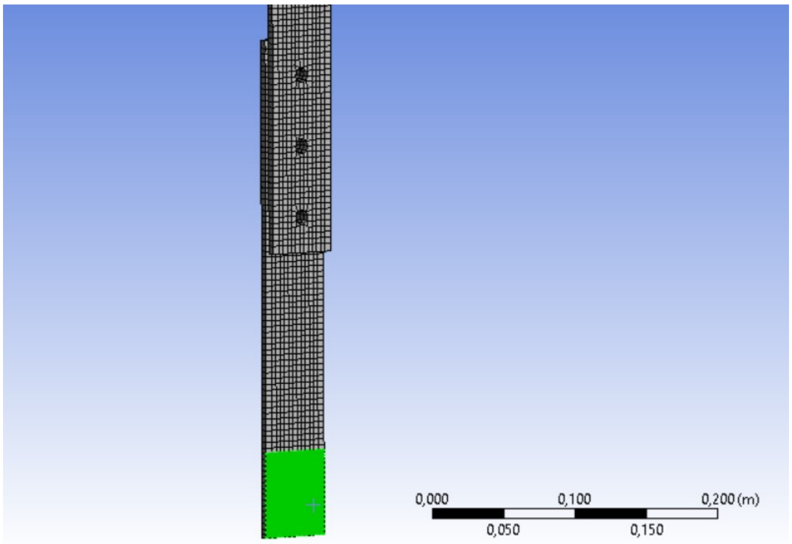

Figure 3.5: Ansys: Simulation of the constraint

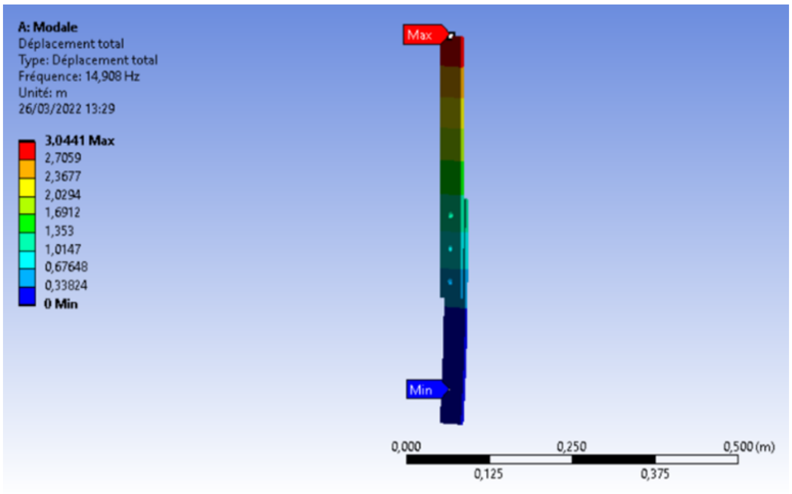

Figure 3.6: First natural frequency

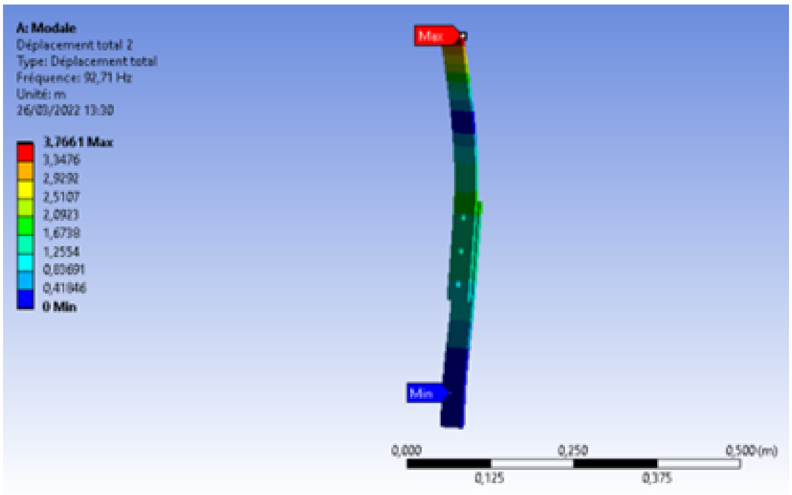

Figure 3.7: Second natural frequency

Mode 1 (Hz)	Mode 2 (Hz)	Mode 3 (Hz)	Mode 4 (Hz)
14,9	92,71	257,39	501

Table 3.1: Ansys simulation results

3.1.2 Experiment frequency sweep

As shown in Table 2.1, four experiments are carried out at a fairly small scanning speed in order to clearly identify and separate the mode shapes of the beam. It can also be noted that, in order to assess the degree of non-linearity of the system, the scanning is

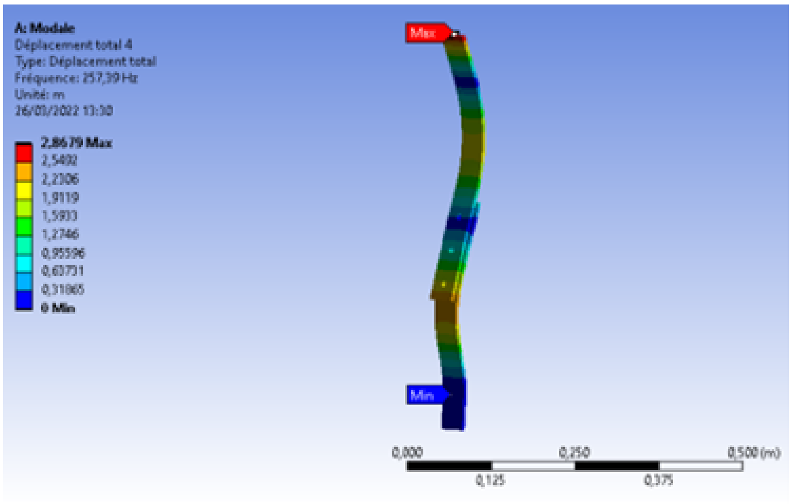

Figure 3.8: Third natural frequency

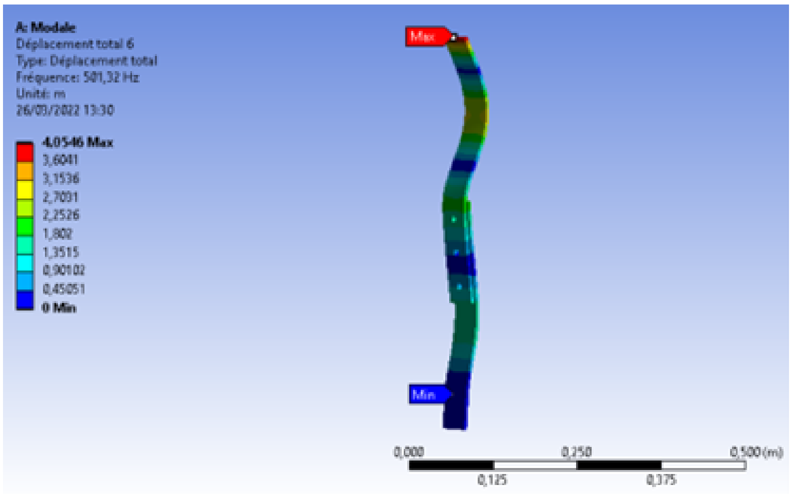

Figure 3.9: Fourth natural frequency

carried out in both increasing and decreasing frequency directions.

The physical reason for this choice is due to the assumption of "non-linearity" of the system; in this case it is necessary to evaluate the spectrum obtained in the two scanning directions because, despite being the same component and so the same system, the results can be very different.

To be more precise an example of spectrum of a non-linear system is shown below:

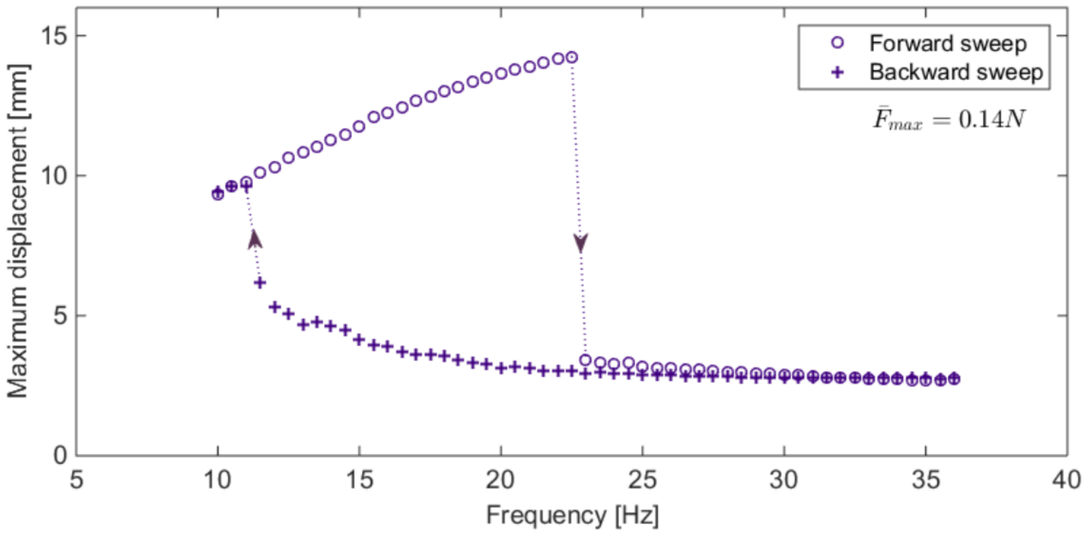

Figure 3.10: Spectrum of a non linear system, [Oscillateur non linéaire à un dégrée de liberté Stefania LO FEUDO, Jean-Luc DION 2021/2022]

The rising sweep is characterised by a very sharp drop after the resonance peak, on the other hand, the descending sweep is characterised by a more gradual rise.

3.1.3 Experimental results

The graphs shown in this section represent the spectrum of the acceleration signal obtained at the free end. Moreover, within the graphs there are two curves, one blue and one red, which refer to the increasing and decreasing frequency sweep respectively.

By zooming in on the peaks of the first mode and the second mode shapes Figure 3.12, it can be seen that for both, the red curves are shifted to the right with respect to the blue curves and this result confirms the non-linearity of the system.

The graph in Figure 3.13 is shown because it can be seen a slight peak at around 900 Hz, but this is completely negligible compared to those obtained at lower frequencies

Mode 1 (Hz)	Mode 2 (Hz)	Mode 3 (Hz)	Mode 4 (Hz)
12,74	71,48	201,3	417,8

Table 3.2: Experimental results

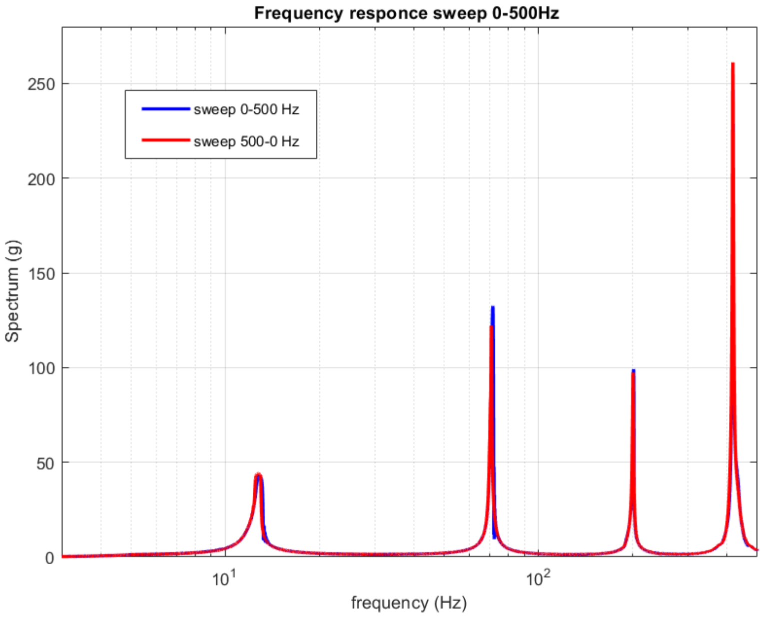

Figure 3.11: Sweep 0-500 Hz

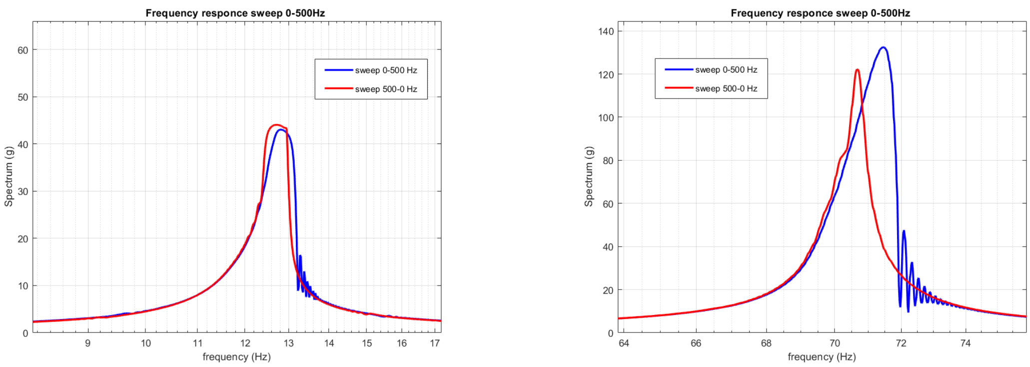

(a) Zoom first natural frequency, Sweep 0-500 Hz

(b) Zoom second natural frequency, Sweep 0-500 Hz

Figure 3.12: Zoom in the peaks

3.1.4 Conclusion: Ansys-Experiment comparison

It can be concluded from the results obtained that **the simulation returns bigger frequency values** than those obtained by simulation for some reasons:

- The simulation model does not include the bolts which, being made of steel, cause a large percentage increase in the weight of the beam, which in the meantime

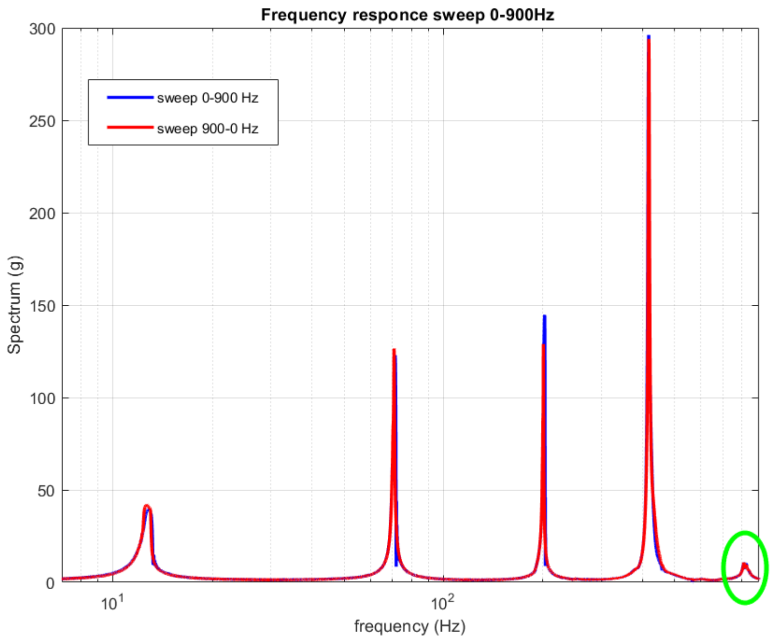

Figure 3.13: Sweep 0-900 Hz

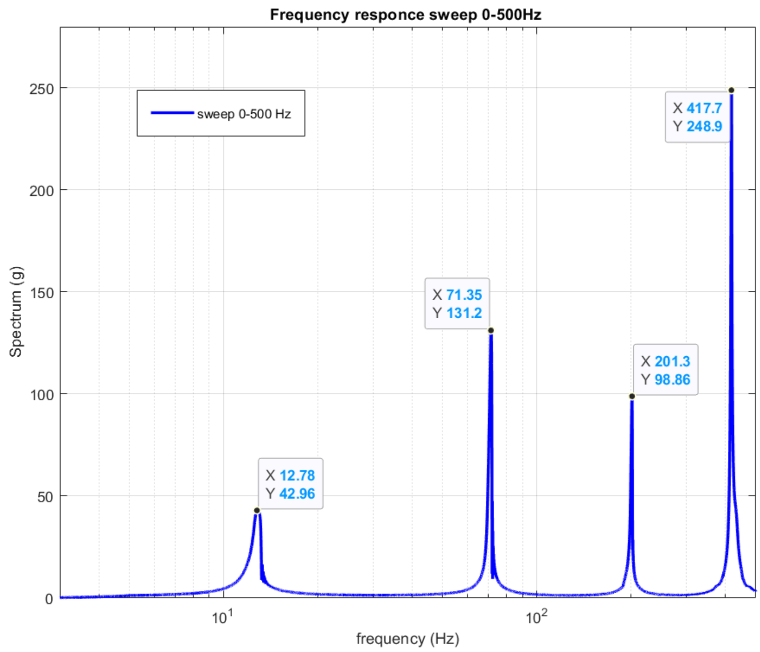

Figure 3.14: Frequency and Module of Acceleration of the mode shapes

-	Mode 1 (Hz)	Mode 2 (Hz)	Mode 3 (Hz)	Mode 4 (Hz)
EXPERIMENT	12,78	71,35	201,3	417,7
ANSYS	14,9	92,71	257,39	501

Table 3.3: Ansys-Experiment comparison

contributes to a change in the resonance frequency of the system (the $\frac{k}{m}$ ratio increases);

- The three-bolt joint simulated on Ansys is a perfect wedge and therefore tends to increase the stiffness of the structure by shifting the frequency response curve on the right;
- The tightening conditions at the interlocking between the base and the beam can never be perfect wedge and therefore this causes a variation in the stiffness of the system.

Note that the effect of resonance frequency variation increases as the excitation frequency of the base increases.

3.2 Experimental results (configurations with dampers)

The results shown in this section refer to the experiments listed in the chapter "**Experimental protocol**" of which the following table is provided:

Configuration	Frequency range (Hz)	octave/minutes	Acceleration
ALL	0-23	0,5	0,8g-1,6g
ALL	55-85	0,5	0,8g-1,6g

Table 3.4: Experiment performed on the 8 configurations

Before showing the results, it is essential to point out that, due to the great sensitivity of the system to variations in experimental conditions, all the curves represented in each graph refer to experimental tests conducted on the same day at a well-defined temperature of the beam maintained around a range of "±5°C" and controlled by the thermocouple Figure 2.9. Therefore, it may not make sense to compare the absolute values of the various graphs with each other, but it is necessary to evaluating the curves in relation to the configuration without dampers present on each graph. Moreover, is recommended to apply a tightening torque of at least 15Nm, as any lower torque could result in unscrewing during the experimental tests.

The effect of varying the tightening torque was evaluated on configuration 1 and led to the results shown in Figure 3.15:

As can be seen from the graph in Figure 3.15, as the tightening torque increases, the curve shifts to the right since at the same time an increase occurs in stiffness and thus the natural resonance frequency of the system increases.

Brief remind of the confgurations:

- **Configuration 1**: Coupling without dampers;
- **Configuration 2**: Coupling with Type1 damper, configuration of 2 dampers, one on each side;
- **Configuration 3**: Coupling with Type 1 damper, configuration of 4 dampers, two on each side, in phase;

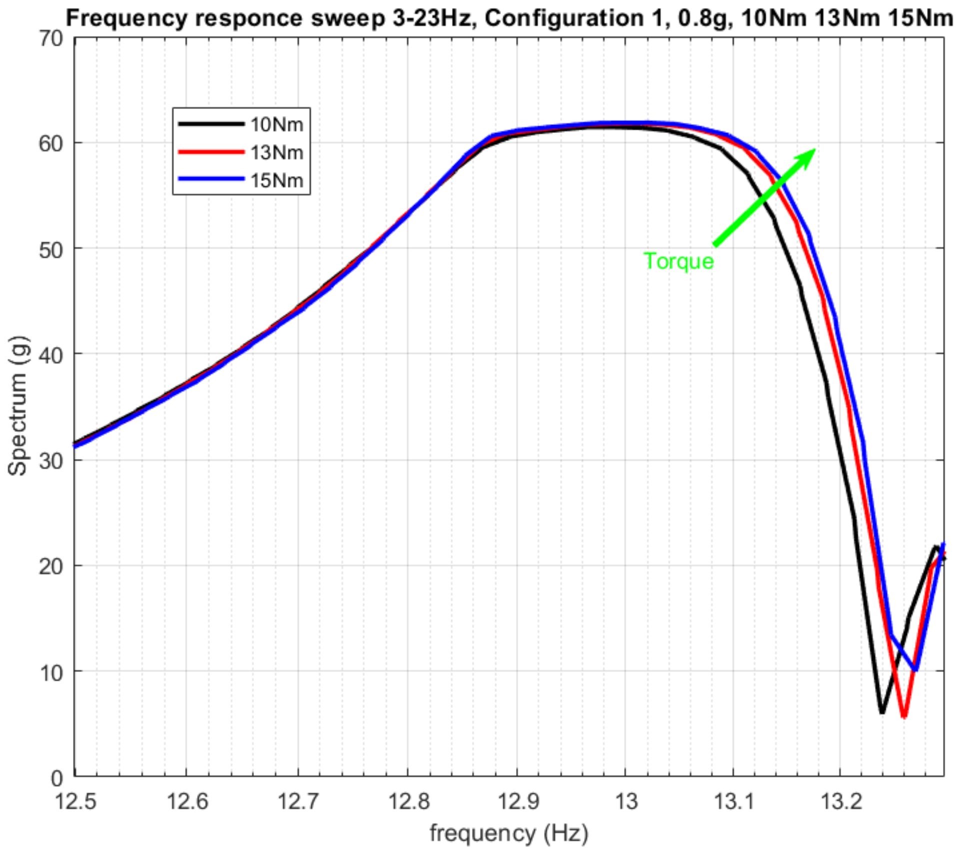

Figure 3.15: Spectrum of Configuration 1 with different tightening torque

- **Configuration 4**: coupling with Type 1 damper, configuration of 4 dampers, two on each side, in counterphase;
- **Configuration 5**: Coupling with Type1 damper, configuration of 4 dampers,two on each side, stacked;
- **Configuration 6**: Coupling with Type 1 damper, configuration of 6 dampers, three on each side, stacked;
- **Configuration 7**: coupling with Type 2 damper, configuration of 3 dampers;
- **Configuration 8**: coupling with Type 3 damper, configuration of 3 dampers;

3.3 Comparison 1

3.3.1 First mode shape, frequency responce, 0,8g

Mode Shape	Configuration	Freqeucy Range (Hz)	Acceleration (g)
1	1,2,3,4	3-23	0,8

Table 3.5: First mode shape, frequency responce, 0,8g

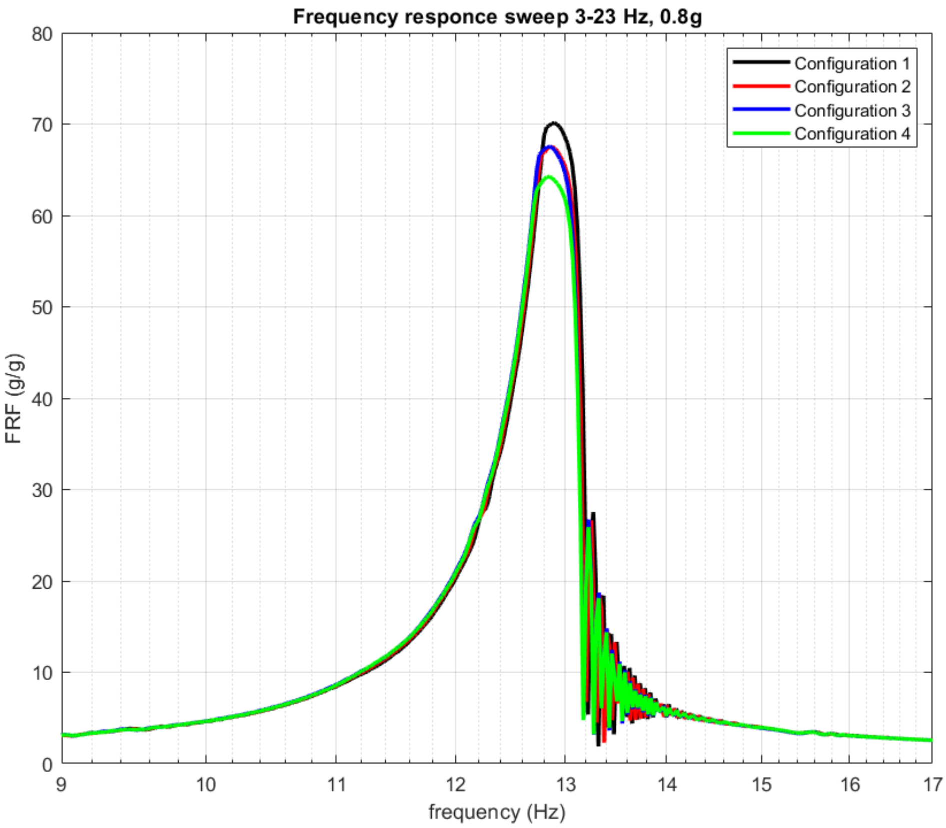

Figure 3.16: First mode shape, frequency responce, 0,8g

3.3.2 First mode shape, frequency responce, 1,6g

Mode Shape	Configuration	Frequecy Range (Hz)	Acceleration (g)
1	1,2,3,4	3-23	1,6

Table 3.6: First mode shape, frequency responce, 1,6g

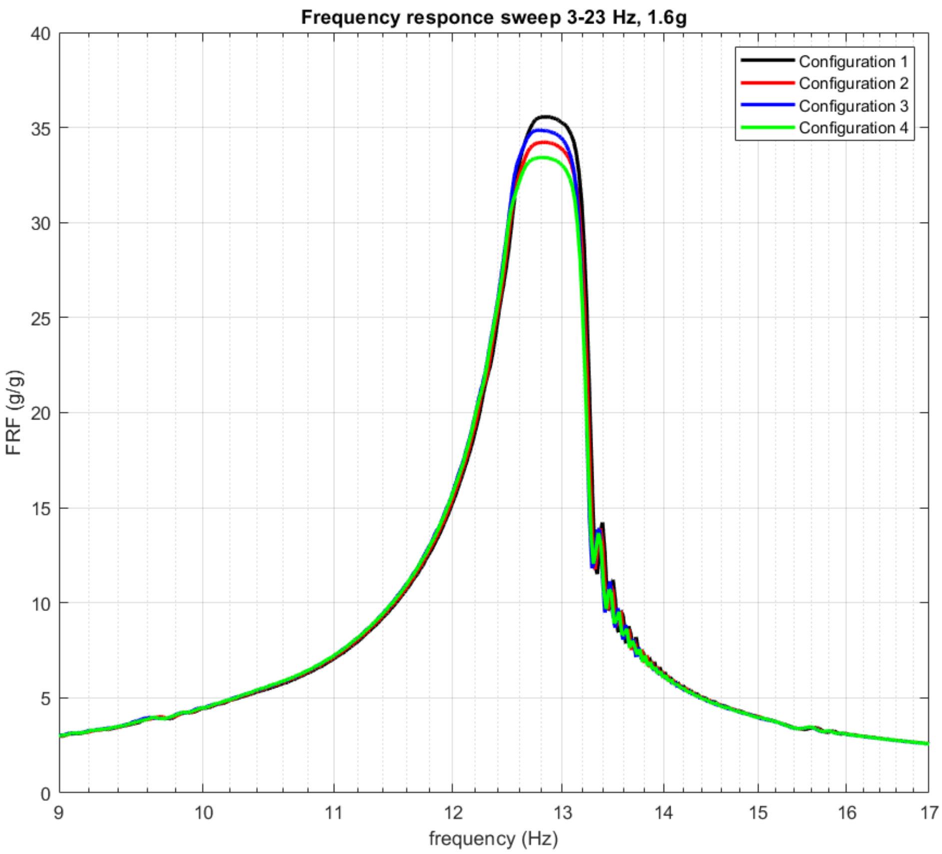

Figure 3.17: First mode shape, frequency responce, 1,6g

3.3.3 Second mode shape, frequency responce, 0,8g

Mode Shape	Configuration	Frequency Range (Hz)	Acceleration (g)
2	1,2,3,4	55-85	0,8

Table 3.7: Second mode shape, frequency responce, 0,8g

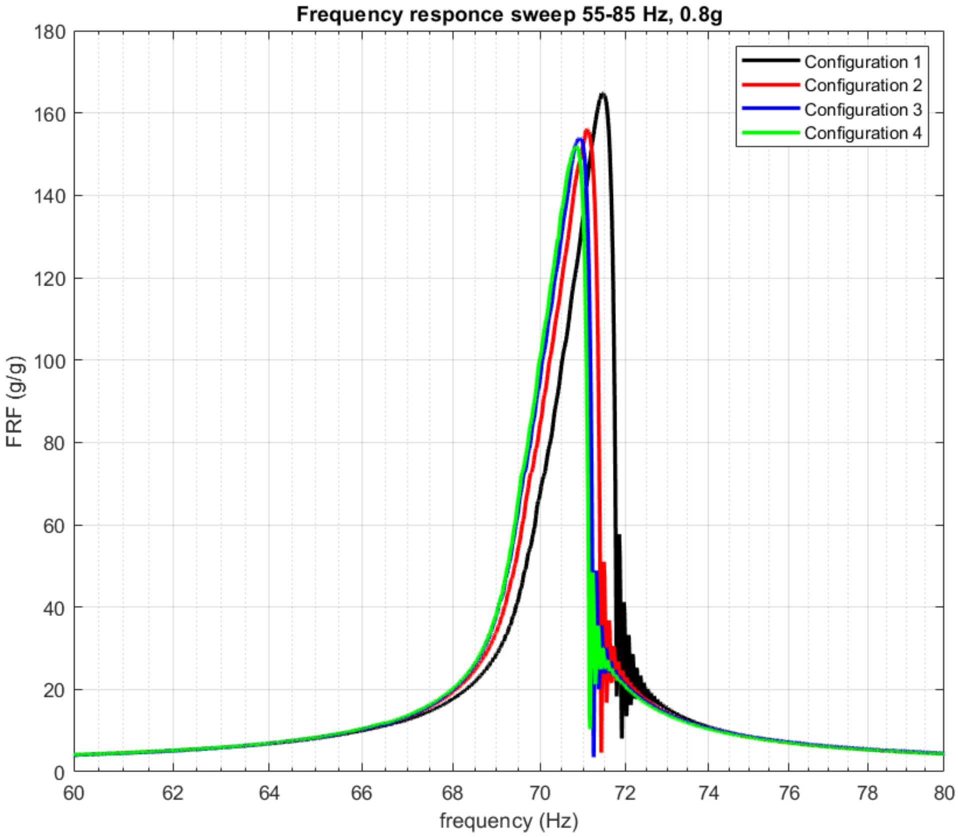

Figure 3.18: Second mode shape, frequency responce, 0,8g

3.3.4 Second mode shape, frequency responce, 1,6g

Mode Shape	Configuration	Frequecy Range (Hz)	Acceleration (g)
2	1,2,3,4	55-85	1,6

Table 3.8: Second mode shape, frequency responce, 1,6g

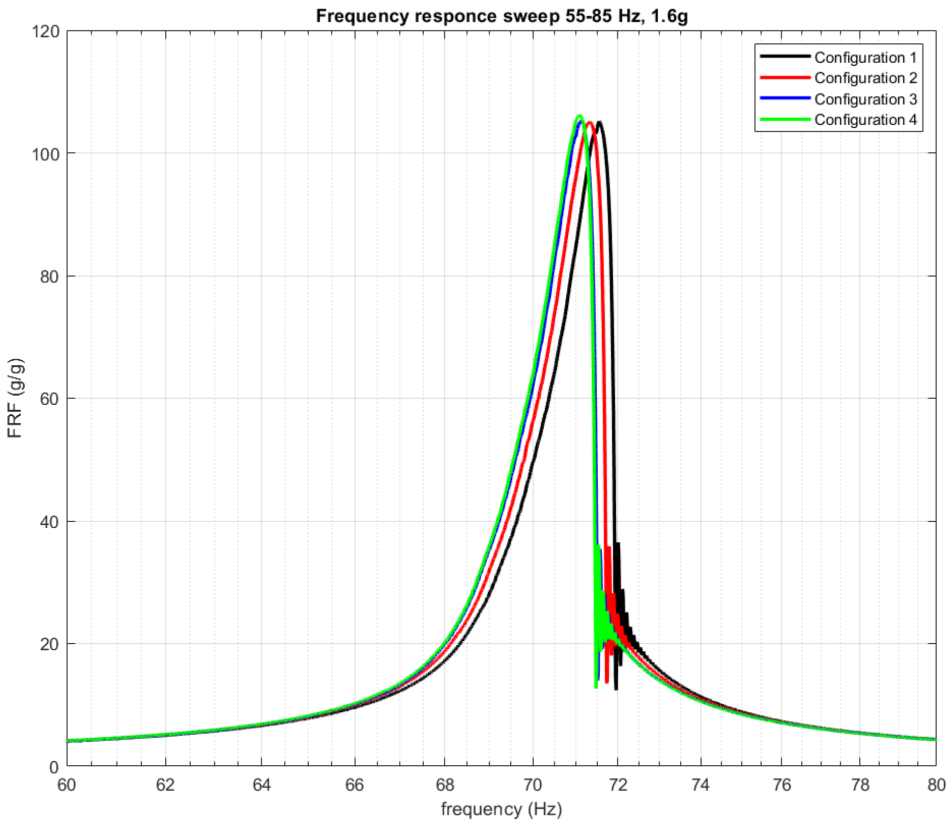

Figure 3.19: Second mode shape, frequency responce, 1,6g

3.3.5 First mode shape (12,8 Hz), Acceleration 0,8g 1,6g

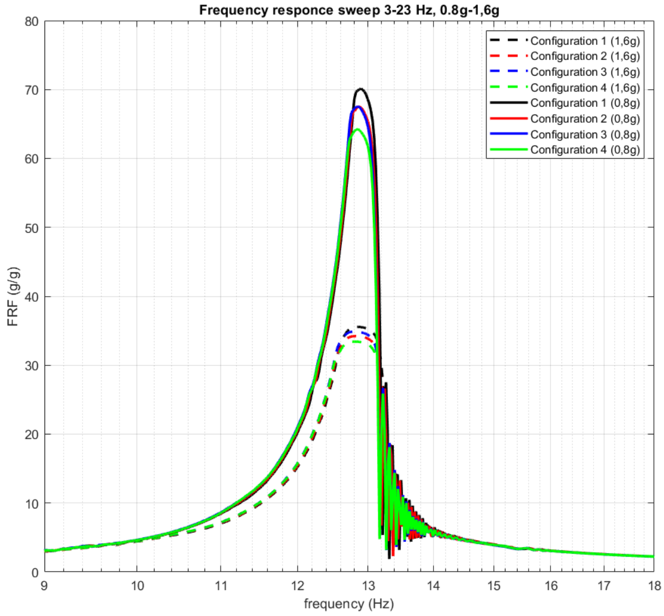

Figure 3.20: Configuration 1,2,3,4, FRF "Mode shape 1" compared under different input excitations (Acc 0,8g-1,6g)

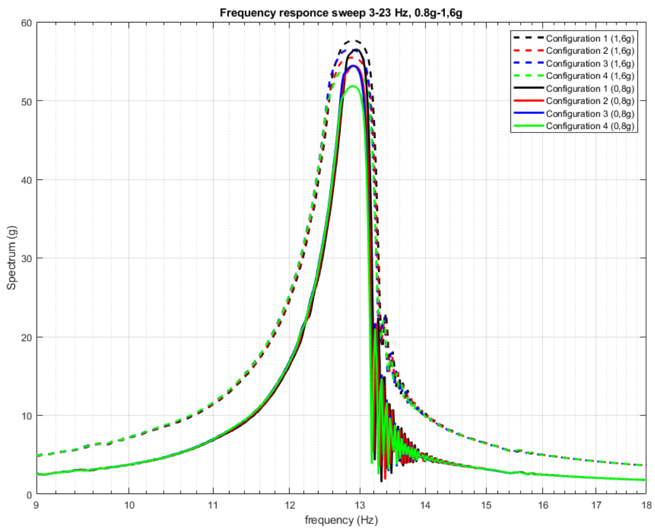

Figure 3.21: Configuration 1,2,3,4, Spectrum "Mode shape 1" compared under different input excitations (Acc 0,8g-1,6g)

3.3.6 Second mode shape (71 Hz), Acceleration 0,8g 1,6g

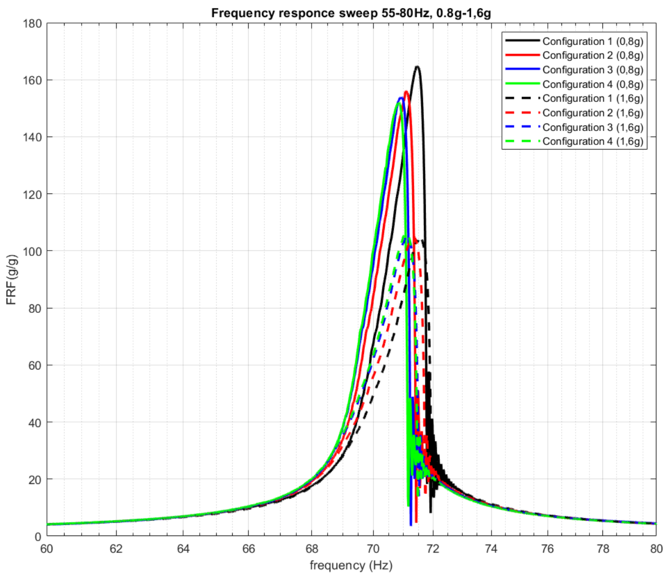

Figure 3.22: Configuration 1,2,3,4, FRF "Mode shape 2" compared under different input excitations (Acc 0,8g-1,6g)

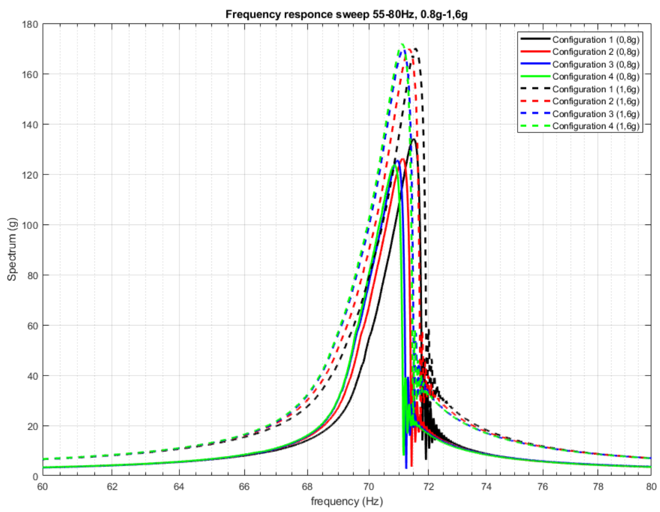

Figure 3.23: Configuration 1,2,3,4, Spectrum "Mode shape 2" compared under different input excitations (Acc 0,8g-1,6g)

3.3.7 Conclusions

From the results obtained, it can be stated that:

- For both vibration modes, a greater decrease in response is obtained by exciting the system with an acceleration of 0.8g;
- The graphs in Figure 3.23 and Figure 3.22 show that the system's response varies as the input changes, and this behaviour is typical of a non-linear system;
- As regards the experiments carried out with an acceleration equal to 1.6g, it is evident that there is a reduction in the resonance frequency rather than a reduction in the response amplitude;
- In all comparisons, except Second mode shape (71 Hz) Acceleration 1.6g 0.2 oct/min, **configuration 4 is the most effective** as it provides the greatest reduction of both resonant frequency and peak response.

3.4 Comparison 2

3.4.1 First mode shape, frequency responce, 0,8g

Mode Shape	Configuration	Frequecy Range (Hz)	Acceleration (g)
1	1,5,6,7,8	3-23	0,8

Table 3.9: First mode shape, frequency responce, 0,8g

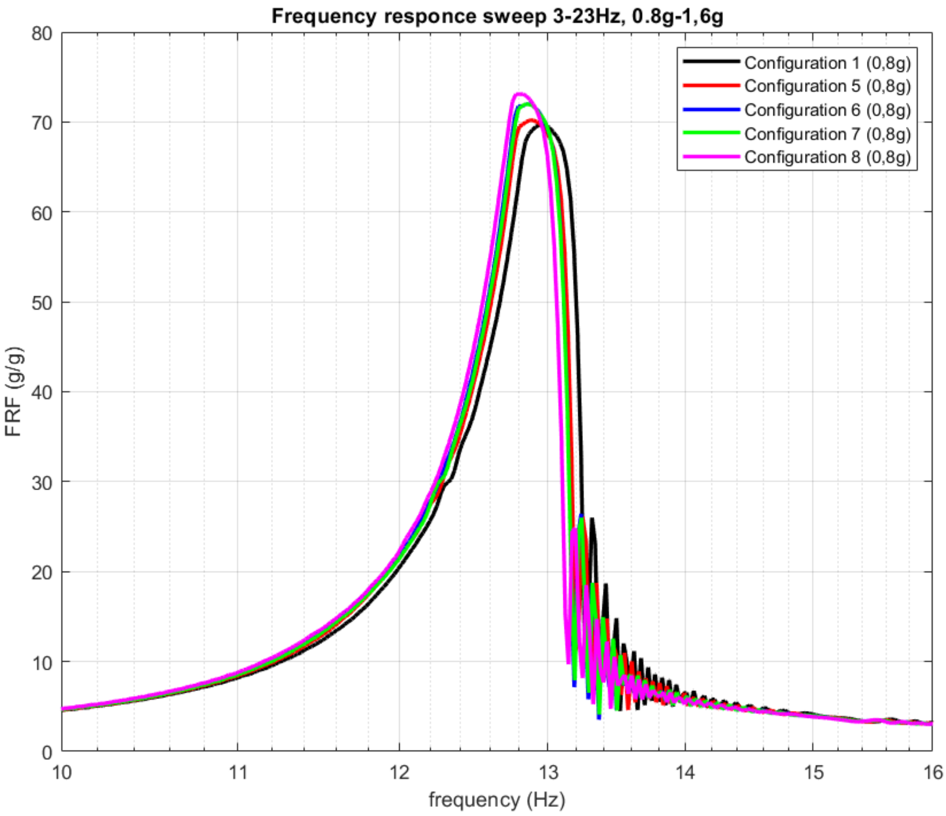

Figure 3.24: FRF first mode shape, frequency responce, 0,8g

3.4.2 First mode shape, frequency responce, 1,6g

Mode Shape	Configuration	Frequecy Range (Hz)	Acceleration (g)
1	1,5,6,7,8	3-23	1,6

Table 3.10: First mode shape, frequency responce, 1,6g

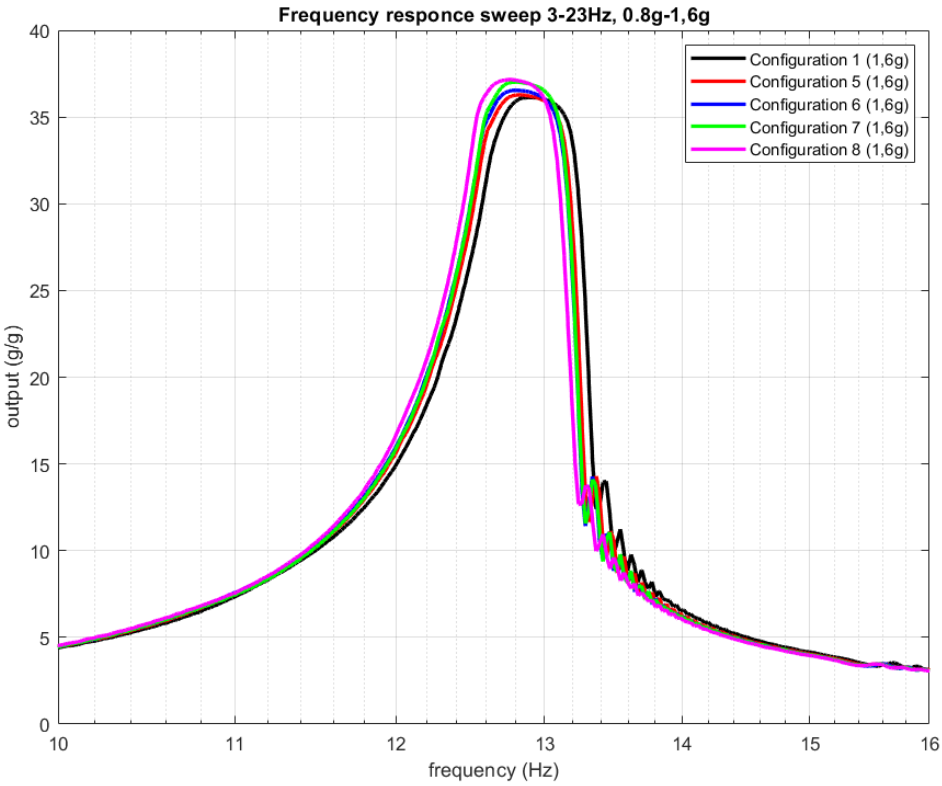

Figure 3.25: FRF first mode shape, frequency responce, 1,6g

3.4.3 Second mode shape, frequency responce, 0,8g

Mode Shape	Configuration	Frequecy Range (Hz)	Acceleration (g)
2	1,5,6,7,8	55-85	0,8

Table 3.11: Second mode shape, frequency responce, 0,8g

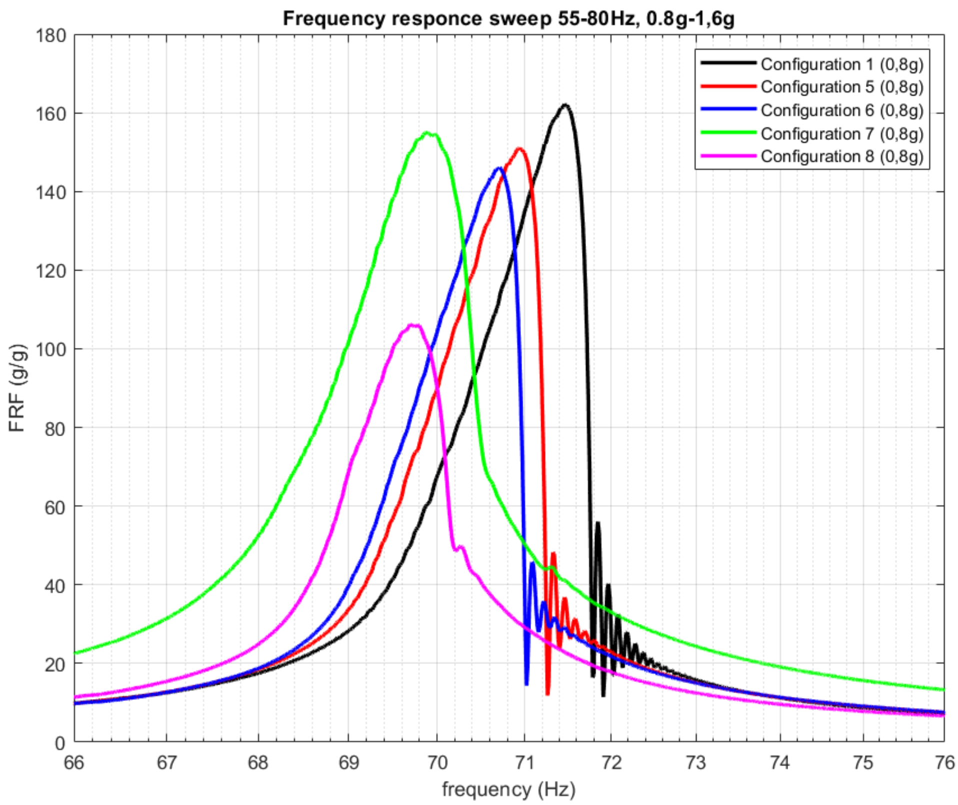

Figure 3.26: FRF second mode shape, frequency responce, 0,8g

3.4.4 Second mode shape, frequency responce, 1,6g

Mode Shape	Configuration	Frequecy Range (Hz)	Acceleration (g)
2	1,5,6,7,8	55-85	1,6

Table 3.12: Second mode shape, frequency responce, 1,6 g

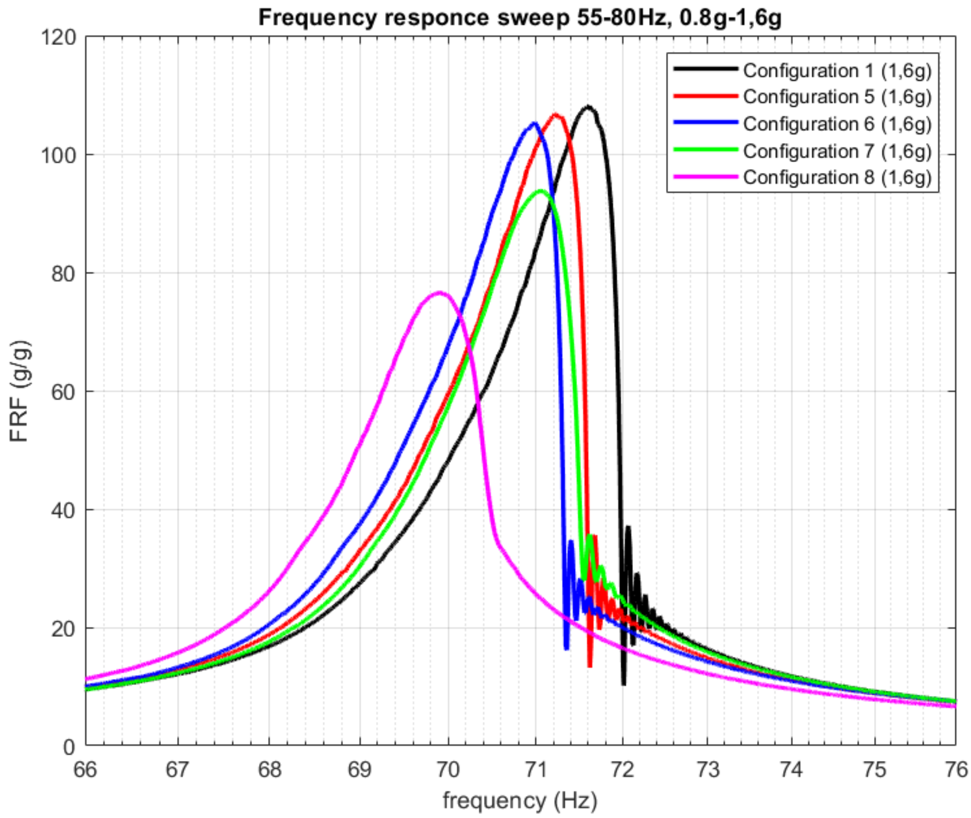

Figure 3.27: FRF second mode shape, frequency responce, 1,6g

3.4.5 First mode shape (12,8 Hz), Acceleration 0,8g-1,6g

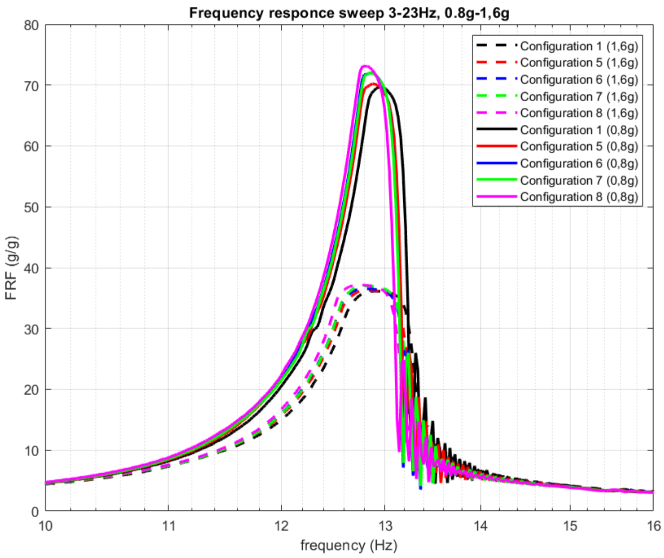

Figure 3.28: Configuration 1,5,6,7,8, FRF "Mode shape 1" compared under different input excitations (Acc 0,8g-1,6g)

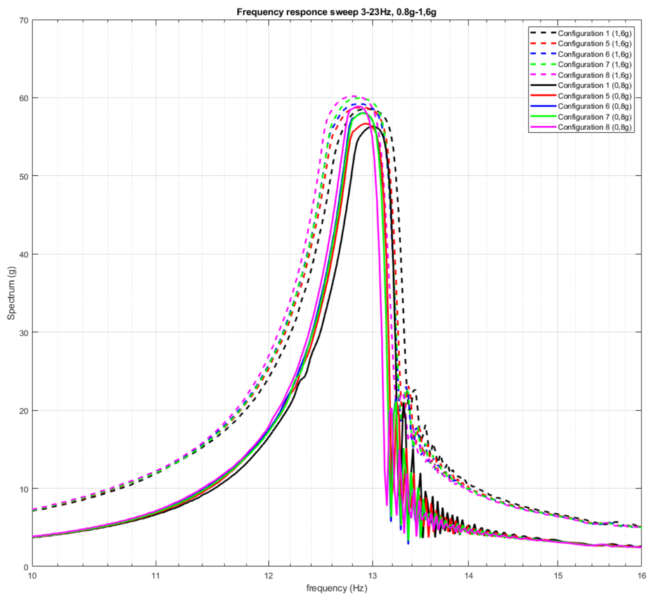

Figure 3.29: Configuration 1,5,6,7,8, Spectrum "Mode shape 1" compared under different input excitations (Acc 0,8g-1,6g)

3.4.6 Second mode shape (71 Hz), Acceleration 0,8g-1,6g

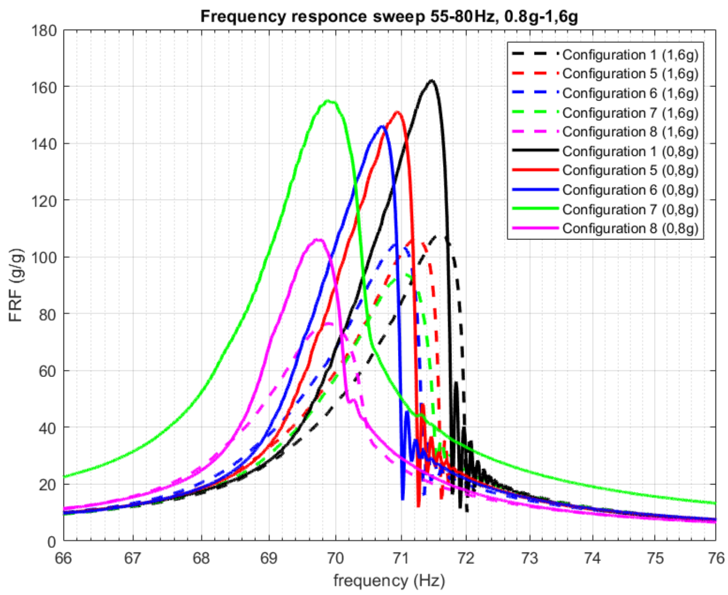

Figure 3.30: Configuration 1,5,6,7,8, FRF "Mode shape 2" compared under different input excitations (Acc 0,8g-1,6g)

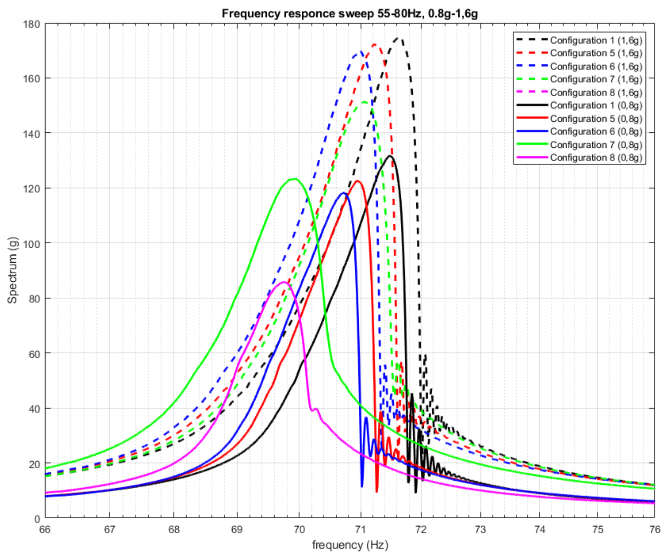

Figure 3.31: Configuration 1,5,6,7,8, Spectrum "Mode shape 2" compared under different input excitations (Acc 0,8g-1,6g)

3.4.7 Conclusions

From the results obtained, it can be stated that:

- Regarding the first mode shape, all the configurations do not have a significant effect on the variation of the FRF peak;
- For the **second mode** shape the **Type 3 damper (configuration 8) is the most effective**, in fact, the FRF peak of the curves obtained with an input of 0.8g and 1.6g are much smaller than the respective responses obtained through the other configurations.

Finally, it can be concluded that the two best configurations are **configuration 4 and configuration 8**.

Post-processing of the data will be performed on these two configurations to extract the modal parameters and thus obtain an estimate of the damping factor.

Chapter 4

Extraction of modal parameters

Introduction

Once the best configurations were chosen, new experiments were performed in order to have further results on which apply the modal parameter extraction methods.

The configurations analysed, in addition to the configuration without damper, are configuration 4 and configuration 8.

The tests were carried out on different days in order to ensure that the shaker worked under the best possible conditions. For each simulation with damper, reference is made to the simulation without the damper carried out on the same day under the most similar working conditions possible.

(a) Configuration 4 (b) Configuration 8

Figure 4.1: Best solutions

Mode shape 1, Configuration 1,4,8

FRF

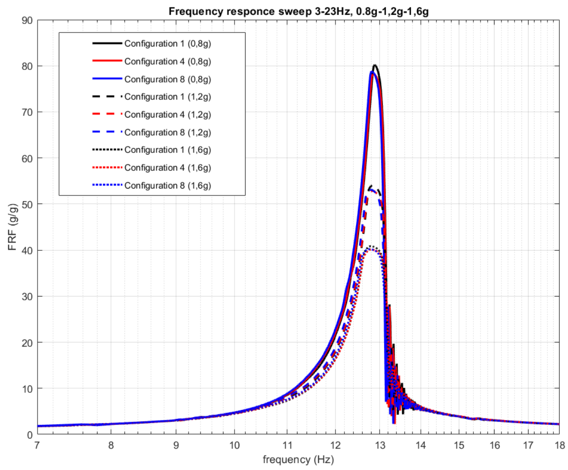

(a) Global result

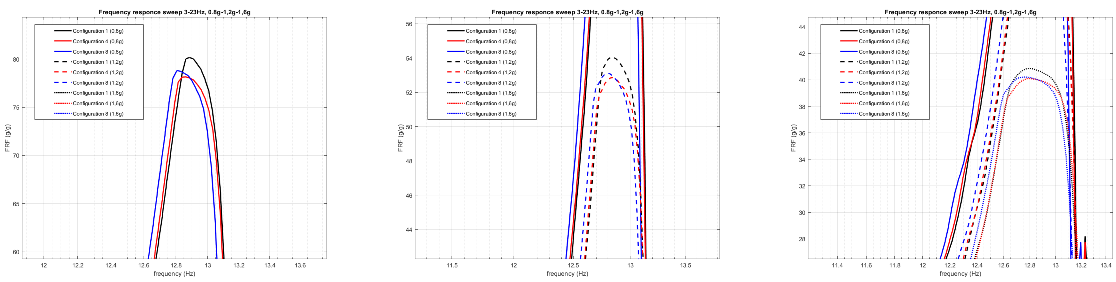

(b) Acceleration 0,8g (c) Acceleration 1,2g (d) Acceleration 1,6g

Figure 4.2: FRF of mode shape 1, configuration 1,4,8

Results

As can be seen from the graphs shown, the reduction in maximum acceleration amplitude due to the presence of the dampers is very small compared to the maximum peak value, so it is possible to conclude that an increase in damping has been achieved, but the effect is not very significant. What can also be confirmed is the repeatability of the results, as the trend of the curves is practically the same for the tests carried out on different days; configuration 4 is the one that provides the best damping effect.

Mode shape 2, Configuration 1,4,8

FRF

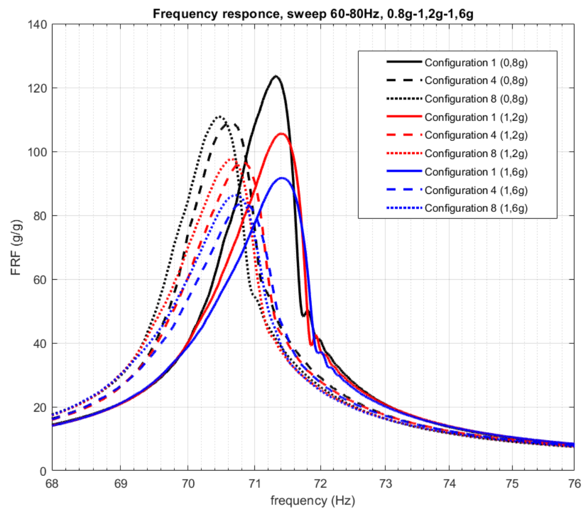

(a) Global result

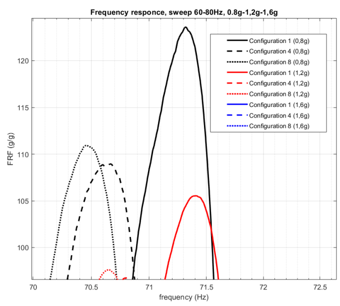

(b) Acceleration 0,8g

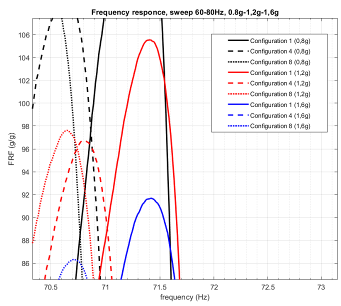

(c) Acceleration 1,2g

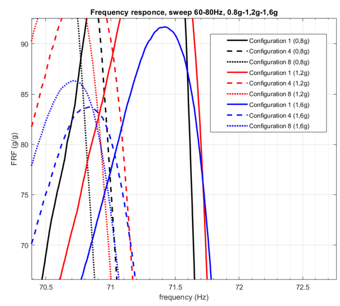

(d) Acceleration 1,6g

Figure 4.3: FRF of mode shape 2, configuration 1,4,8

Results

The experiments performed on the second mode shape are particularly interesting, as it can be seen that as the input acceleration varies and the configuration changes, both the maximum acceleration amplitude and the resonance frequency vary considerably. Again, configuration 4 provides maximum peak reduction.

4.1 "-3dB" Method

Introduction

The first method used to obtain a damping estimate is the so-called '**-3dB method**' or 'power halving method'.

It should be noted that this method gives an exact estimate of the damping when the system is linear and the FRF curve is perfectly symmetrical. In the case studied, the system is not perfectly linear and in fact the spectrum is not symmetrical with respect to the resonance frequency. However, there are methods that can be used for non-linear systems that allow, through a small correction, a more accurate estimate of the damping while using the -3dB method [6]. To apply the method, the spectrum (output only) and the FRF (output/input) was taken into account. To have an idea of the non-linearity of the system and how the damping factor was evaluated, an example of the calculation performed for configuration 1, on the second mode shape, is presented below:

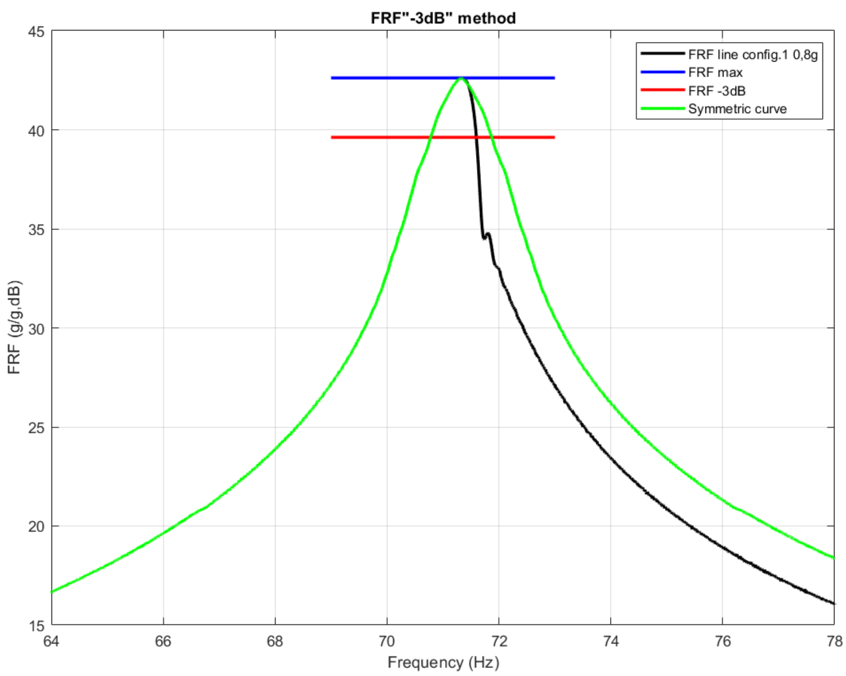

Figure 4.4: FRF mode shape 2, configuration 1, "-3dB" Method, 0,8g

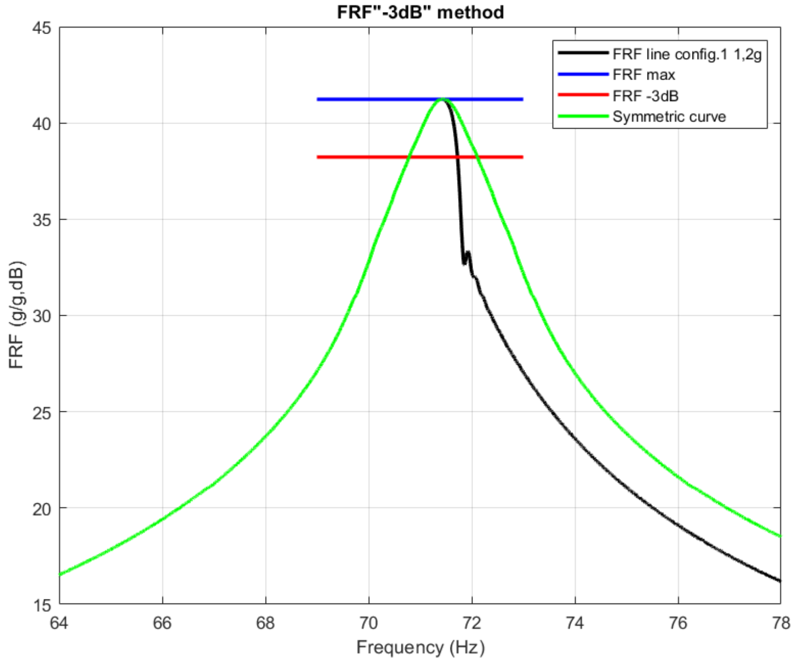

Figure 4.5: FRF mode shape 2, configuration 1, "-3dB" Method, 1,2g

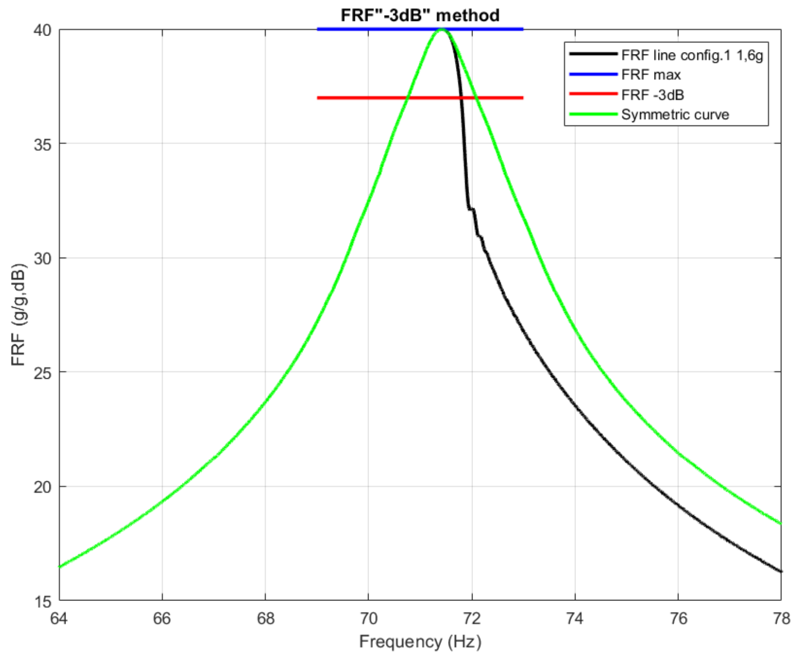

Figure 4.6: FRF mode shape 2, configuration 1, "-3dB" Method, 1,6g

The damping factor was obtained using the canonical formula of the '-3dB' method Equation 4.1, and two other formulas suggested in the literature [6] in which corrections are applied to account for the non-linearity of the system:

$$\zeta_1 = \frac{(\omega_2 + \omega_1)(\omega_2 - \omega_1)}{2\omega_{res}^2} \tag{4.1}$$

$$\zeta_2 = \frac{(\omega_2^2 - \omega_1^2)(1+p)}{(\omega_2^2 + \omega_1^2)\sqrt{\frac{1}{r^2} - 1}} \tag{4.2}$$

$$\zeta_3 = \frac{\sqrt{\frac{1+rp}{1+p}}(\omega_2 - \omega_1)}{\omega_{res}} \tag{4.3}$$

Where:

- r is the factor equal to $\sqrt{2}$ for the *-3dB* method
- p is the term for the correction factor which can be obtained by means of the following graph in Figure 4.7 (A value of $p = 0.02$ was taken into account in the calculation.)

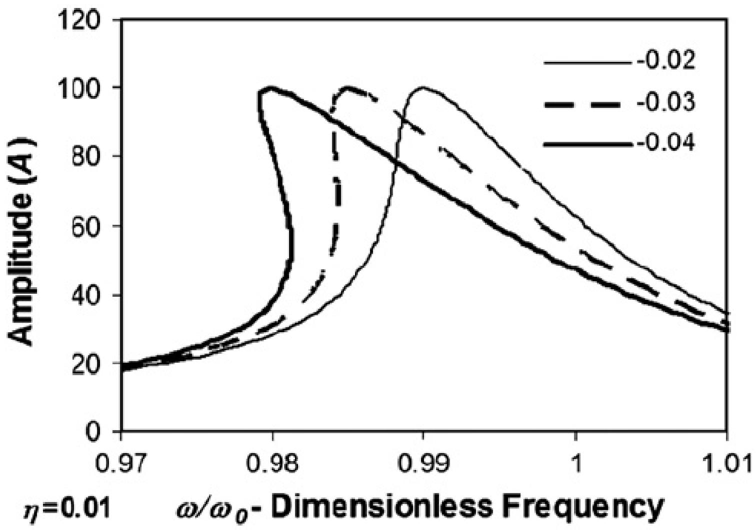

Figure 4.7: Typical graphs obtained for different values of the p coefficient [6]

4.1.1 Results

The result of the calculation performed on both vibration modes of the beam for the three configurations and for the three different input excitation levels is shown in Table 4.1, Table 4.2, Table 4.3, Table 4.4.

Mode Shape 1 "Spectrum"	Acceleration (g)	ζ_1	ζ_2	ζ_3
Configuration 1	0,8	3,5%	3,61%	3,5%
	1,2	4,5%	4,62%	4,5%
	1,6	5,4%	5,54%	5,4%
Configuration 4	0,8	3,7%	3,76%	3,7%
	1,2	4,7%	4,87%	4,7%
	1,6	5,8%	5,95%	5,8%
Configuration 8	0,8	3,7%	3,8%	3,7%
	1,2	4,6%	4,73%	4,6%
	1,6	5,6%	5,72%	5,6%

Table 4.1: Mode shape 1 "Spectrum", Damping ratio, 0,8g-1,2g-1,6g

Mode Shape 1 "FRF"	Acceleration (g)	ζ_1	ζ_2	ζ_3
Configuration 1	0,8	2,59%	2,64%	2,59%
	1,2	2,03%	2,09%	2,04%
	1,6	1,98%	2,03%	1,98%
Configuration 4	0,8	2,58%	2,63%	2,58%
	1,2	1,77%	1,82%	1,78%
	1,6	1,96%	2,01%	1,96%
Configuration 8	0,8	2,5%	2,59%	2,52%
	1,2	1,9%	1,95%	1,9%
	1,6	1,8%	1,89%	1,81%

Table 4.2: Mode shape 1 "FRF, Damping ratio, 0,8g-1,2g-1,6g

Mode Shape 2 "Spectrum"	Acceleration (g)	ζ_1	ζ_2	ζ_3
Configuration 1	0,8	1,15%	1,18%	1,15%
	1,2	1,3%	1,33%	1,3%
	1,6	1,45%	1,48%	1,45%
Configuration 4	0,8	1,32%	1,35%	1,32%
	1,2	1,41%	1,45%	1,41%
	1,6	1,56%	1,59%	1,56%
Configuration 8	0,8	1,25%	1,28%	1,25%
	1,2	1,38%	1,41%	1,38%
	1,6	1,50%	1,54%	1,50%

Table 4.3: Mode shape 2, "Spectrum", Damping ratio, 0,8g-1,2g-1,6g

Mode Shape 2 "FRF"	Acceleration (g)	ζ_1	ζ_2	ζ_3
Configuration 1	0,8	1,14%	1,17%	1,14%
	1,2	1,31%	1,33%	1,31%
	1,6	1,44%	1,47%	1,43%
Configuration 4	0,8	1,30%	1,33%	1,30%
	1,2	1,41%	1,44%	1,41%
	1,6	1,56%	1,60%	1,56%
Configuration 8	0,8	1,25%	1,28%	1,25%
	1,2	1,37%	1,40%	1,37%
	1,6	1,51%	1,55%	1,51%

Table 4.4: Mode shape 2, "FRF", Damping ratio, 0,8g-1,2g-1,6g

Conclusions

From the results in the tables, it can be observed that the damping values obtained by applying the method to the spectrum of the first mode shape are much higher than those obtained by applying the method to the FRF of the first mode shape. The FRF, in fact, was purposely evaluated with respect to the accelerometer placed at the interlocking in order to filter out the response from the effect of the base damping.

The reason could be due to the fact that the first mode shape is strongly influenced by the presence of the constraint and therefore by the damping contribution of the base (hence the reason for the higher values); there are some technical guidelines that even prohibit the use of the first mode shape for the determination of the damping factor and in this case there is good evidence in the discrepancy of the results. A relevant point is that the result obtained using Equation 1 and Equation 3 is exactly the same even though Equation 3 is written taking into account the correction factor p.

Concerning the second mode shape, the results obtained by applying the method to the spectrum and FRF are quite similar.

The fact that the system is non-linear can be deduced from the fact that as the excitation level changes for each configuration, the value of the damping factor changes, and so, in order to assess the greatest increase in the damping factor, the average is taken for each configuration.

The highest factor increase is achieved with configuration 4, and the result is following:

Mode Shape 2	ζ_{avg}
Configuration 1	1,30%
Configuration 4	1,43%
$\Delta\zeta$	10%

Table 4.5: Mode shape 1, Damping ratio, 0,8g-1,2g-1,6g

Therefore, it can be concluded that through the *'-3dB'* method, the estimated damping increase is **10%**. It must be noted that the difficulties experienced in applying the "-3dB" method are various, and in particular one must take into account the fact that the spectrum signal rather than the FRF obtained in the laboratory is the result of approximations due to the conversion from analogue to digital and from time domain to the frequency domain through a Fourier Transform. This can result in an error in the determination of the resonance peak with a consequent error in finding the two frequencies at -3dB. Furthermore, to obtain a more precise estimate, one would have to perform several calculations by changing the dB number, but this is not always feasible, especially if the curve is not perfectly symmetrical.

In a case like the one studied, it might also be a good solution to adopt a different method of extracting modal parameters in order to be able to compare the results and have a better estimate of the damping factor.

4.2 "Dahl" method

Introduction

As already mentioned in chapter 1, Dahl's method is a very effective method for estimating the damping contribution generated by friction. In this case, in fact, it does not deal with viscous damping, but with hysteretic damping, obtained through energy dissipation due to relative motion between two surfaces. To evaluate the equivalent viscous damping factor, the literature [2] suggests to consider the hysteresis cycle areas that identify the energy dissipated and the work of the external force due to the friction between the dampers and the beam.

In detail:

$$\eta_{eq} = \frac{E_{diss}}{\pi W_{ext}} \tag{4.4}$$

Where, as can be seen in Figure 4.8 :

- E_{diss} corresponds to an half of the hysteresis loop area (blue one);
- W_{ext} corresponds to the maximum stored elastic energy "$0.5 \cdot F_{max} \cdot x_{max}$" (red one).

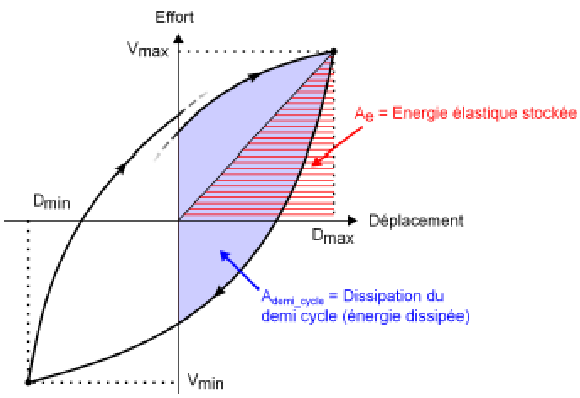

Figure 4.8: Hystereic cycle [2]

Moving more specifically into the schematisation of the system, since the experiments were carried out imposing as input the displacement of the base of the beam, a forced harmonic oscillator subjected to base excictation has been taken into account as a model. One of the first steps in determining the damping factor is to find an analytical model that can simplify the real system.

The beam we are dealing with can be schematised as follows (Figure 4.9), since the joint can be supposed as "n" springs in parallel,

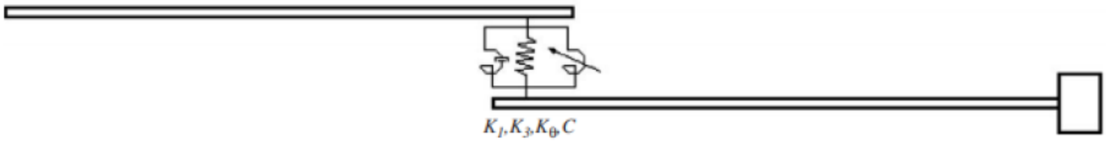

Figure 4.9: Beam scheme [1]

and therefore, since the system input is a horizontal sine sweep, a reasonable model could be the mass-spring-damper system forced by a base displacement:

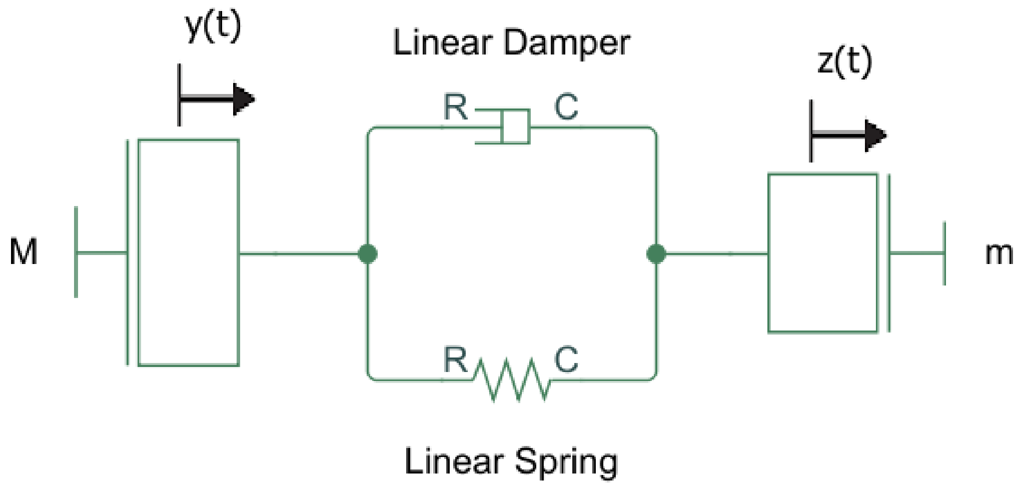

Figure 4.10: Mass-Spring-Damper system

The generic equation of motion the mass "m" fot this kind of system (Figure 4.10) can be written as follows:

$$m\ddot{z} + c\dot{z} + kz = ky \tag{4.5}$$

Where, referring to the real system :

- **m** is the modal mass;

- **k** is the modal stiffness;
- $\ddot{z}$ is the acceleration of the free end;
- **z** is the displacement of the free end;
- **y** is the displacement of the base;
- $\mathbf{c\dot{z}}$ is the dissipating term which, referred to the Dahl model, corresponds to the friction force F_f.

So, the final equation of the system (Figure 4.11) can be written as:

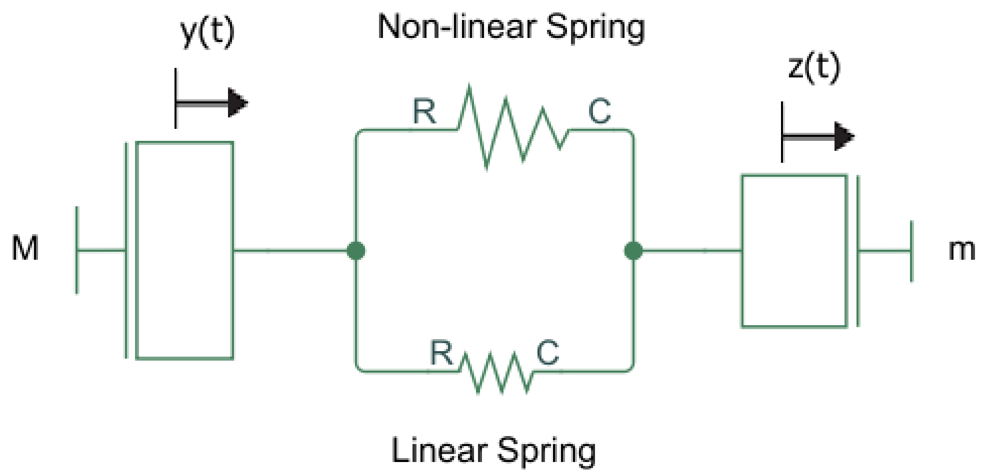

Figure 4.11: Mass-Spring-Non-Linear Spring system

$$m\ddot{z} + F_f + kz = ky \tag{4.6}$$

The objective to be achieved is to know the trend of the force F_f as a function of the displacement z, since the graphical representation of this is precisely the hysteresis loop which allows the damping factor to be determined. About the Equation 4.6 the only known term is the acceleration $\ddot{z}$ (as it was acquired during the experiments).

In order to determine the force F_f, one must first evaluate the modal mass and modal stiffness, the displacement x and the displacement y, and at this point, it is possible to isolate the friction force F_f and evaluate its trend as a function of displacement z.

$$F_f = ky - m\ddot{z} - kz \tag{4.7}$$

Extraction of Modal Mass and Modal Stiffness

In order to evaluate the modal mass and modal stiffness, configuration 1 of the beam was considered and two experiments were performed for each mode shape, imposing two different boundary conditions on the beam.

The first experiment was carried out as usual, exciting the system in the frequency range close to resonance, thus obtaining a result practically equal to those obtained from the experiments carried out previously; the second experiment was carried out within the same frequency range, but positioning a mass of 57g at the free end.

(a) (b)

Figure 4.12: Position of the added masss

The result of the two experiments is necessarily different, as the addition of the mass causes a decrease in the ratio $\frac{k}{m}$ and thus a decrease in the resonance frequency compared to the original configuration.

Assuming the modal stiffness constant in the two experiments, it is possible to solve a system of two equations in two unknowns, where the unknowns are the modal mass and modal stiffness, known the two resonance frequencies from the frequency response function graph and the value of the added mass.

The system of equations is the following:

$$\begin{cases} f_1 = \sqrt{\frac{k}{m}} \\ f_2 = \sqrt{\frac{k}{m+\Delta m}} \end{cases} \tag{4.8}$$

with $\Delta m = 57g$

Moreover, to have an idea of the accuracy of the experimental results, a simulation was carried out on Abaqus to evaluate the resonance frequencies of the beam in the two configurations (with and without mass in the free end) for the first and second modes shapes.

4.2.1 Result Mode shape 1

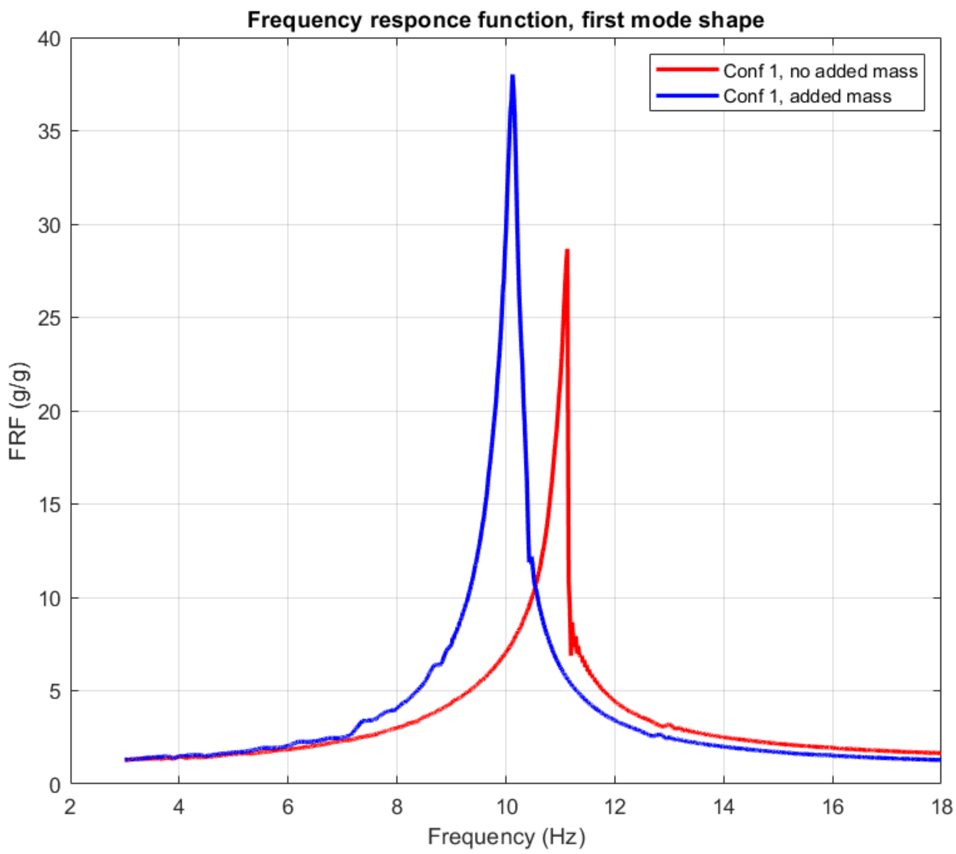

Figure 4.13

The Abaqus simulation results are shown in figure:

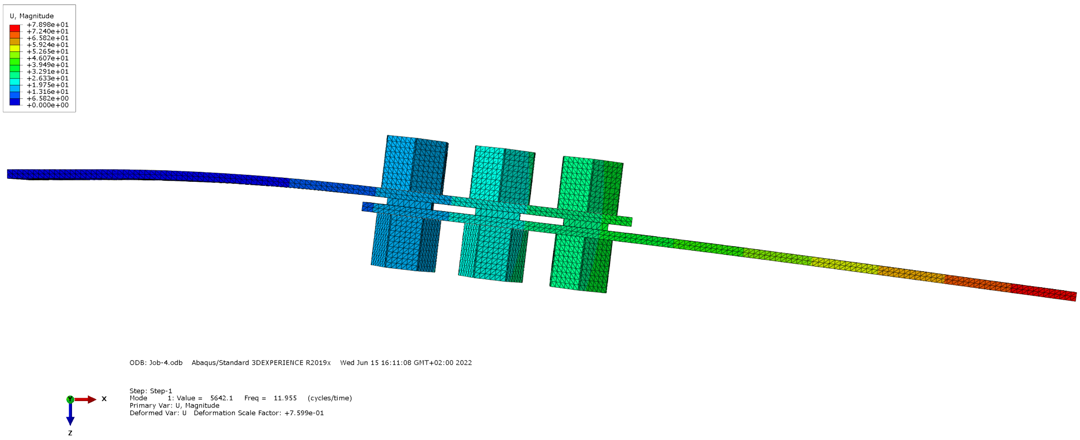

Figure 4.14: Mode shape 1 without added mass

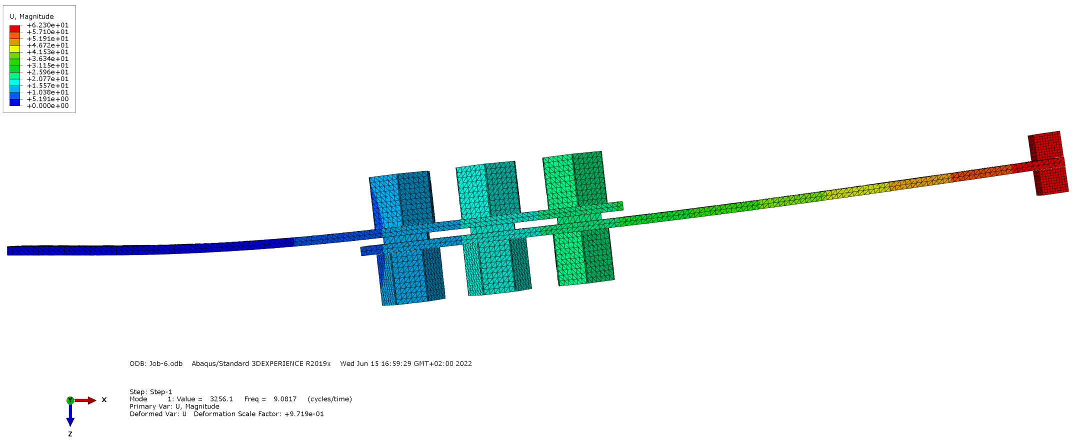

Figure 4.15: Mode shape 1 with added mass

Modal mass and modal stiffness values have been derived from the following system of equations

$$\begin{cases} f_1 = \sqrt{\frac{k}{m}} \\ f_2 = \sqrt{\frac{k}{m+\Delta m}} \end{cases} \tag{4.9}$$

-	Added Mass	Frequecy (Hz)	**Modal mass (kg)**	**Modal stiffness** ($\frac{N}{m}$)
Experiment	NO	11.12	0.306	$1.4 \cdot 10^3$
Abaqus	NO	11.955	0.078	$0.4 \cdot 10^3$
Experiment	YES	10.20	0.306	$1.4 \cdot 10^3$
Abaqus	YES	9.0817	0.078	$0.4 \cdot 10^3$

Table 4.6: First mode shape

4.2.2 Result Mode shape 2

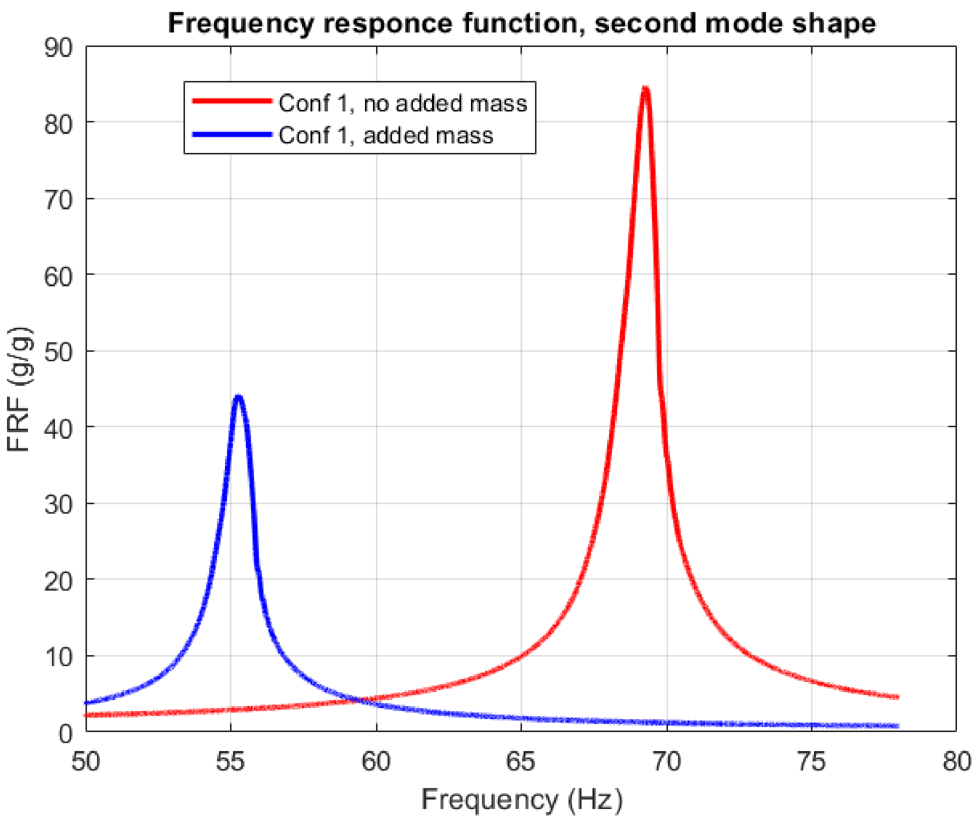

Figure 4.16

The Abaqus simulation results are shown in figure:

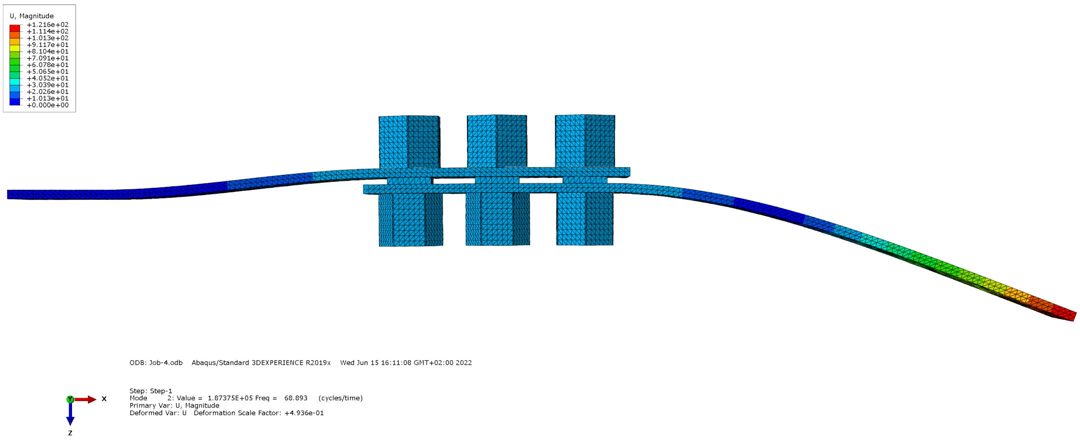

Figure 4.17: Mode shape 2 without added mass

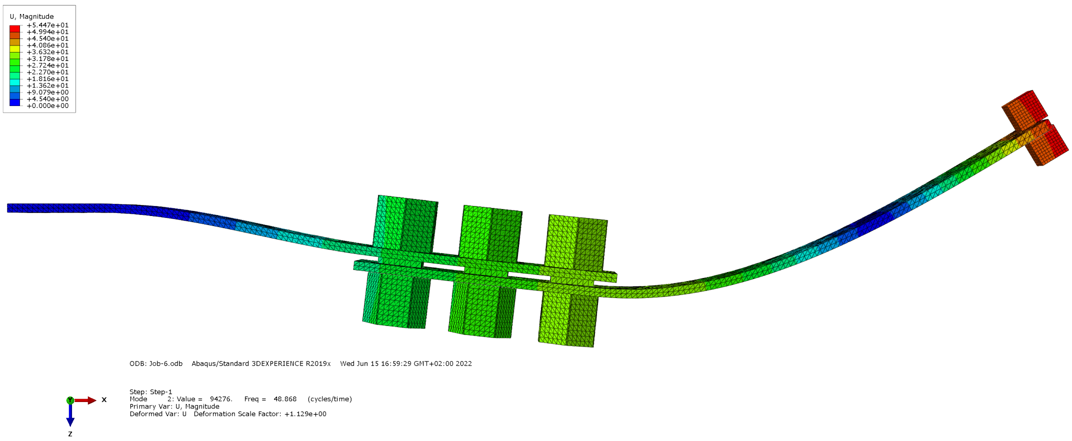

Figure 4.18: Mode shape 2 with added mass

Modal mass and modal stiffness values have been derived from the following system of equations:

$$\begin{cases} f_1 = \sqrt{\frac{k}{m}} \\ f_2 = \sqrt{\frac{k}{m+\Delta m}} \end{cases} \tag{4.10}$$

-	Added Mass	Frequecy (Hz)	**Modal mass (kg)**	**Modal stiffness ($\frac{N}{m}$)**
Experiment	NO	69.2	0.101	$1.9 \cdot 10^4$
Abaqus	NO	68.893	0.058	$1 \cdot 10^4$
Experiment	YES	55.2	0.101	$1.9 \cdot 10^4$
Abaqus	YES	48.868	0.058	$1 \cdot 10^4$

Table 4.7: Second mode shape

4.2.3 Displacement computation

At that point, knowing the mass and modal stiffness for the two mode shapes, to derive the force expression F_f you must derive the displacement z of the free end and the displacement of the base.

Considering a generic experiment of those performed, the calculation of the base and free end displacement as a function of time must be based on the acceleration signal.

Actually, considering the acceleration signal locally as a sinusoidal signal with constant amplitude and frequency, displacement and acceleration differ from each other by a constant equal to ω^2, where ω is the angular frequency of oscillation of the system. This solution could be obtained by solving the following generic system of equations:

$$\begin{cases} x(t) = x_0 e^{i\omega t} \\ \dot{x}(t) = i\omega x_0 e^{i\omega t} \\ \ddot{x}(t) = -\omega^2 x_0 e^{i\omega t} \end{cases}$$

From the first and third equations it's possible to obtain the desired formula:

$$\ddot{x}(t) = -\omega^2 x(t) \tag{4.11}$$

To obtain the value of ω in the time interval considered, it is sufficient to know the sampling frequency, which in the experiments performed is known and equal to 2048 Hz, the number of periods taken into account and the total number of points of the interval.

The reason why it was possible to assume that the acceleration is a sinusoidal signal with constant frequency and amplitude is due to the fact that, given the low sweep speed

(0.5 octave/min for the first mode shape and 0.2 octave/min for the second mode shape), selecting a sufficiently small number of oscillations, the signal respects the assumptions already made.

A problem to be solved in order to make the above assumptions as close as possible to the real condition, is related to the noise due to the higher order frequencies. As can be seen from the image in Figure 4.20a, in fact, at the resonance peak a lot of noise perturbs the signal and therefore in order to attenuate it a low pass filter at 120 Hz was used.

The filtered signal assumes the shape in Figure 4.20b and Figure 4.20d and thus, selected an appropriate number of periods, the initial assumptions of constant frequency and amplitude of oscillations are valid.

The graphs in Figure 4.19 show the effect of the low-pass filter applied to the free end acceleration signal.

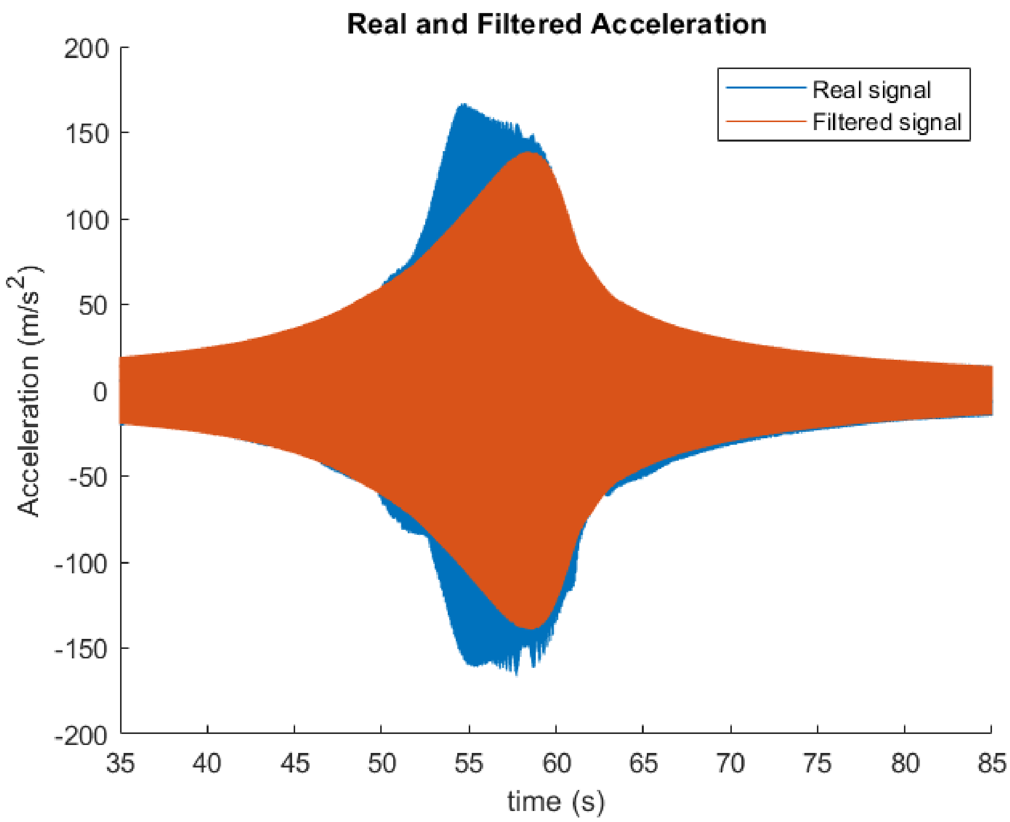

Figure 4.19: Low pass filter effect, configuration 8

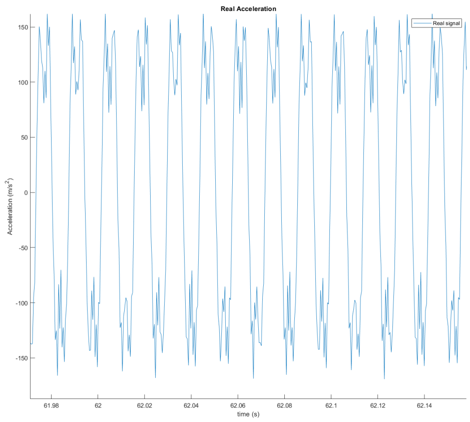

(a) Real free end Acceleration

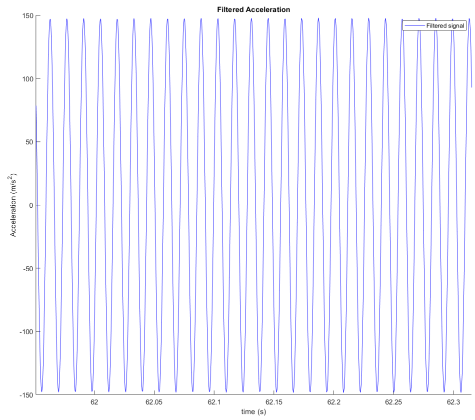

(b) Filtered free end Acceleration

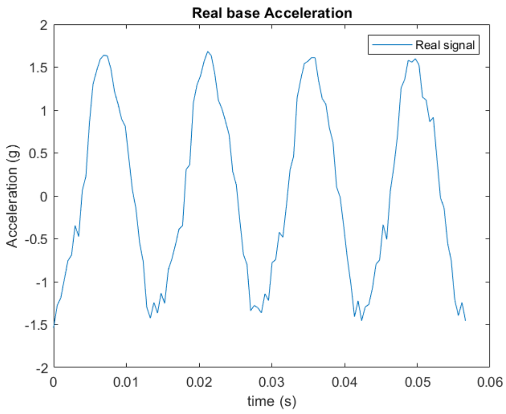

(c) Real base Acceleration

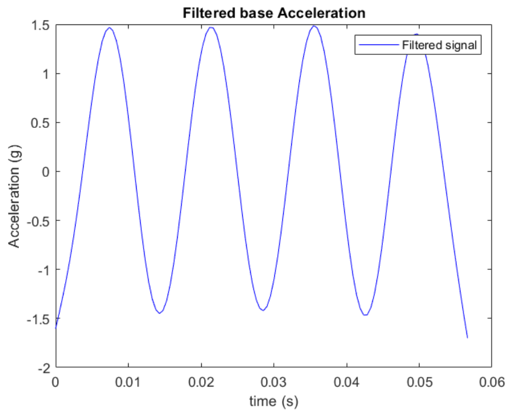

(d) Filtered base Acceleration

Figure 4.20: Real and filtered Acceleration

The results will be presented in the following order:

- **Configuration 1**: Free end acceleration and free end position, base acceleration and base position (Figure 4.21 and Figure 4.22);
- **Configuration 4**: Free end acceleration and free end position, base acceleration and base position (Figure 4.23 and Figure 4.24);
- **Configuration 8**: Free end acceleration and free end position, base acceleration and base position (Figure 4.25 and Figure 4.26).

Configuration 1

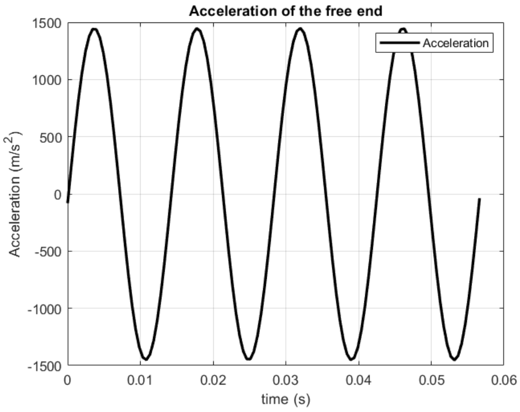

(a) Acceleration free end

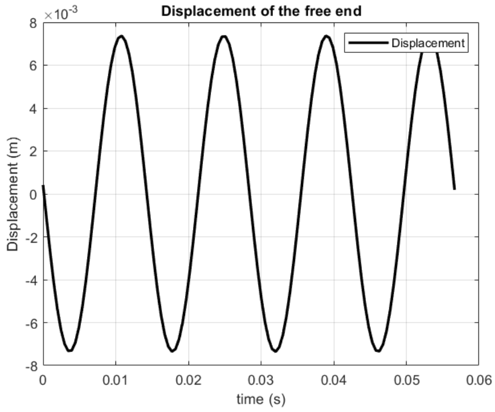

(b) Position free end

Figure 4.21: Free end coordinate 1

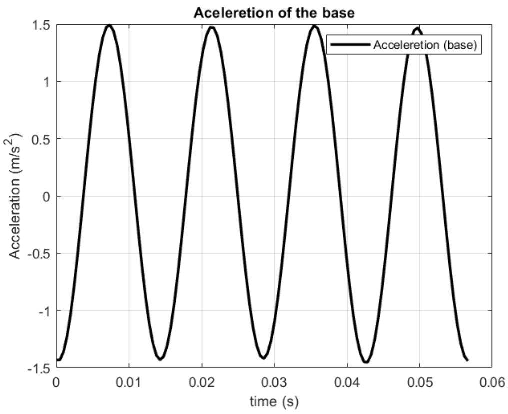

(a) Acceleration of the base

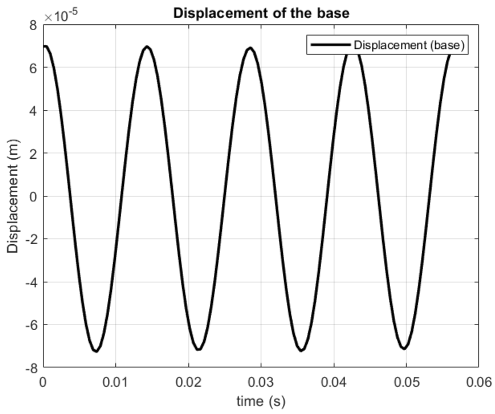

(b) Position of the base

Figure 4.22: Base coordinate 1

Configuration 4

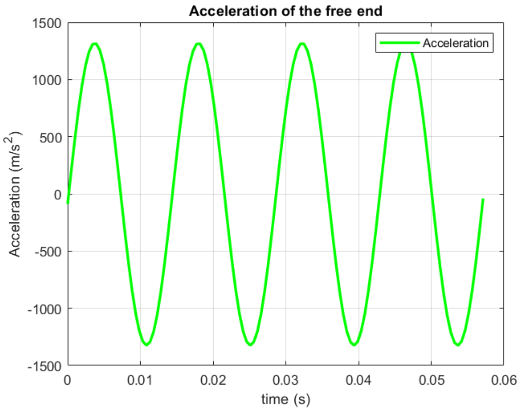

(a) Acceleration free end

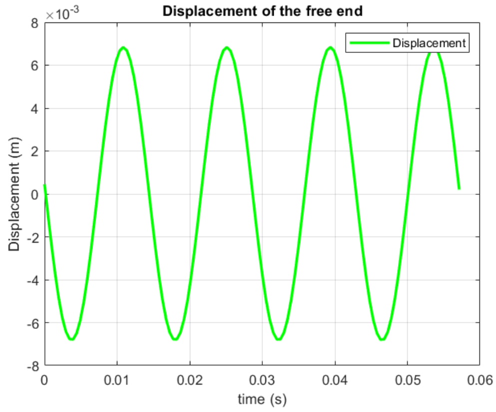

(b) Position free end

Figure 4.23: Free end coordinate 4

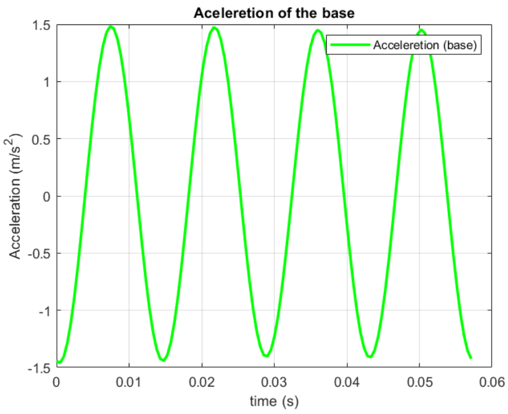

(a) Acceleration of the base

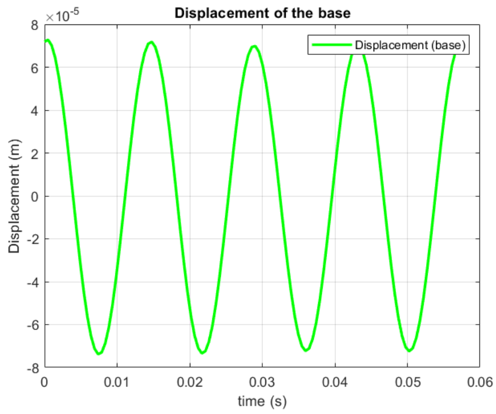

(b) Position of the base

Figure 4.24: Base coordinate 4

Configuration 8

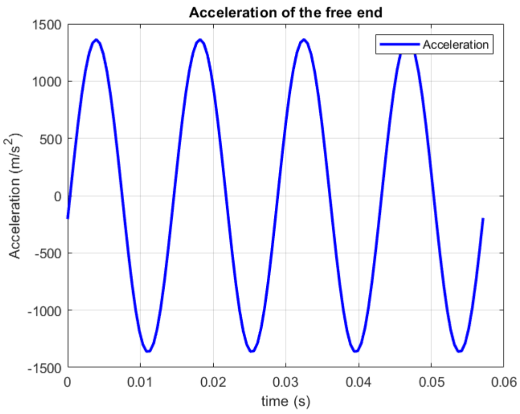

(a) Acceleration free end

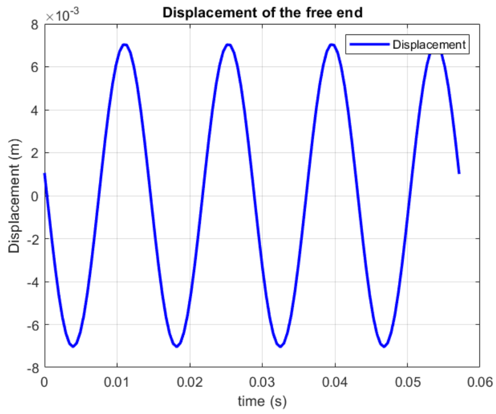

(b) Position free end

Figure 4.25: Free end coordinate 8

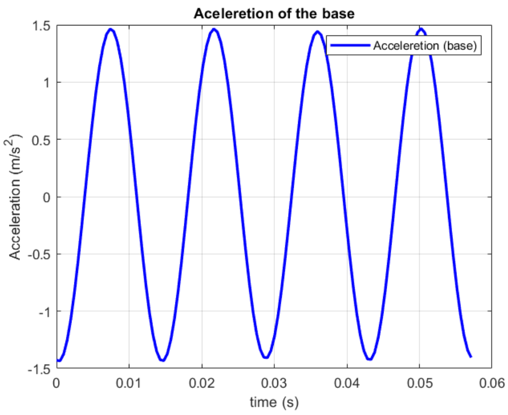

(a) Acceleration of the base

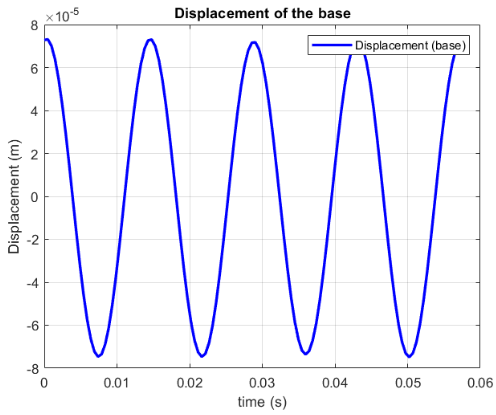

(b) Position of the base

Figure 4.26: Base coordinate 8

4.2.4 Computation of the damping factor

At that point, knowing the modal mass, modal stiffness, acceleration and displacements, it is possible to calculate, for each configuration, the force F_f as a function of the displacement z.

It should be noted that the damping factor was only estimated for the second mode shape, as the simplification of the system in Figure 4.11 is only valid in the case of small oscillations. The first mode shape is characterised by a large free end displacement and therefore the modelling of a base excitation is meaningless for it.

Below are represented the hysteresis cycles for the three configurations obtained considering a modal stiffness of $1.9 \cdot 10^4 \frac{N}{m}$

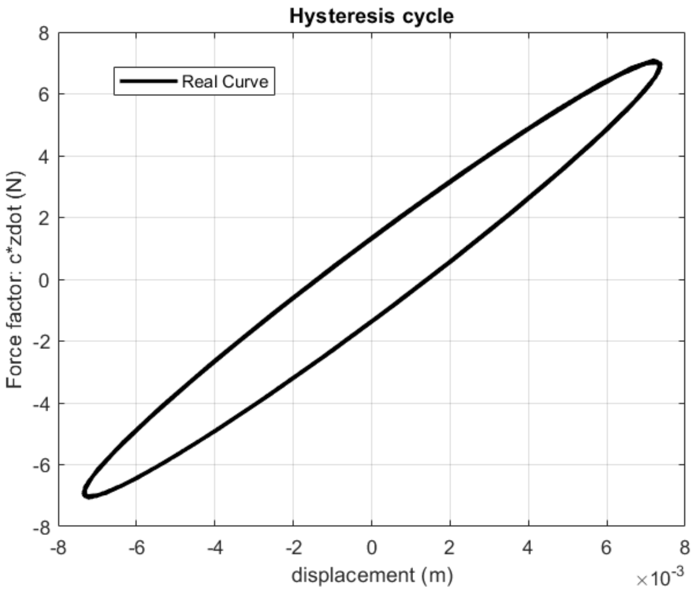

Figure 4.27: Hysteresis cycle Conf. 1

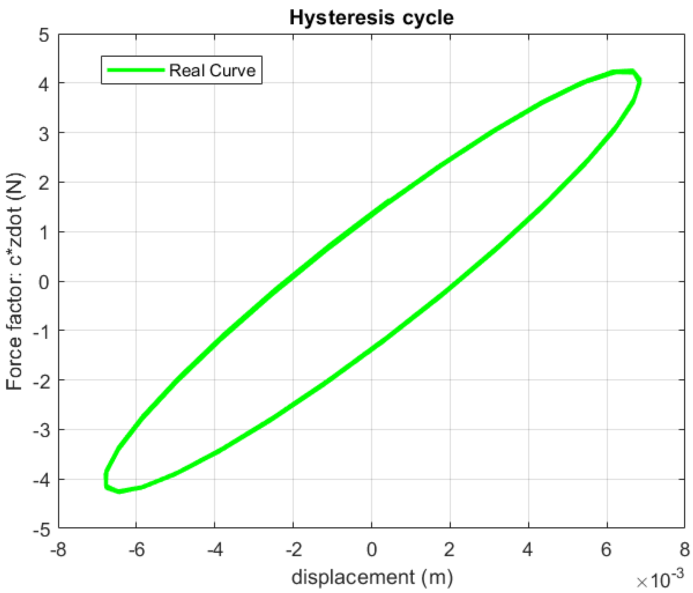

Figure 4.28: Hysteresis cycle Conf. 4

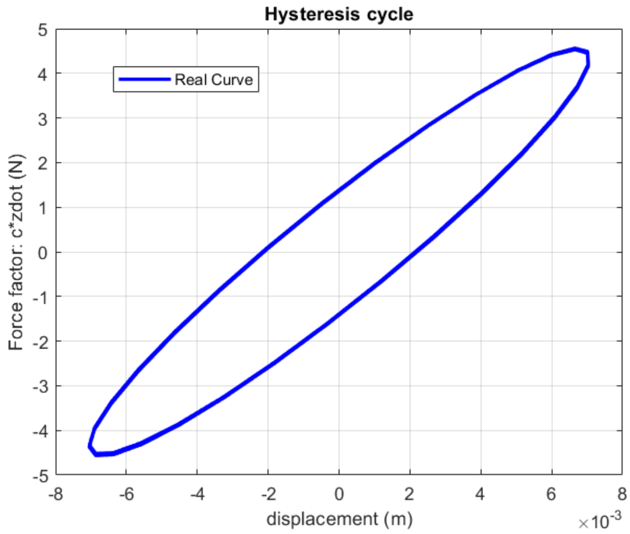

Figure 4.29: Hysteresis cycle Conf. 8

The final calculation of the damping factor has taken into account the great sensitivity of the system to varying modal stiffness. From Table 4.7 it can be seen that the real and numerical modal stiffness values are significantly different. For this reason, in a first step, it was decided to average the damping value obtained when the stiffness varies in the range of values between the real and numerical value. The result is shown in Figure 4.30.

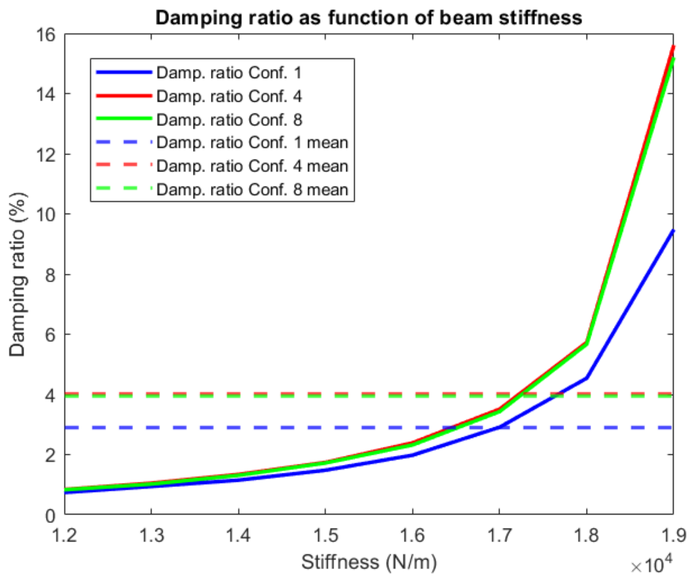

Figure 4.30: Average of damping ratios between minimum and maximun modal stiffness

Configuration	Modal stiffness ($\frac{N}{m}$)	η_{avg}
1	$1.7 \cdot 10^4$	2.91%
4	$1.72 \cdot 10^4$	3.67%
8	$1.72 \cdot 10^4$	3.58%

Table 4.8: Average damping ratio

At that point, by intersecting each mean value with the related curve, the new range to average the three curves was set. In particular, the average was performed into a range of stiffness between $1.7 \cdot 10^4 \frac{N}{m}$ and $1.72 \cdot 10^4 \frac{N}{m}$. The result is shown in Figure 4.31.

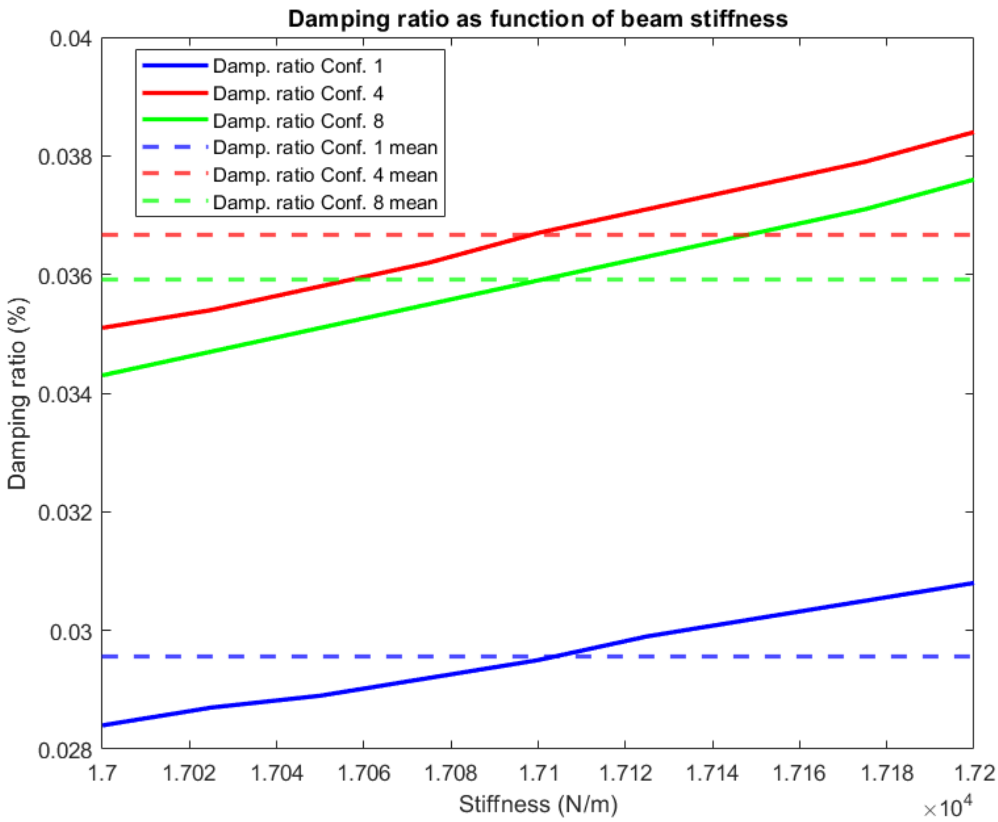

Figure 4.31: Average damping factor for a value of modal stiffness between $1.7 \cdot 10^4 \frac{N}{m}$ and $1.72 \cdot 10^4 \frac{N}{m}$

Within the new range, $\Delta\eta_{avg}$ was evaluated between configuration with damper and without damper.The result is shown in Figure 4.32 and as can be read from the graph, the $\Delta\eta$ corresponds to 24.04% for configuration 4 and 21.5% for configuration 8.

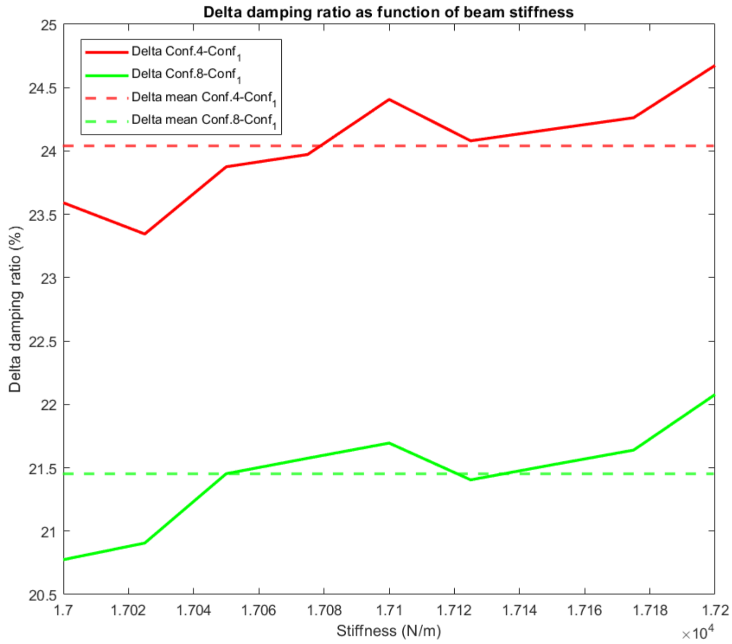

Figure 4.32: $\Delta\eta_{avg}$

Results

Mode Shape 2	η_{avg}	$\Delta\eta_{avg}$
Configuration 1	2.96%	-%
Configuration 4	3.67%	24.04%
Configuration 8	3.59%	21.5%
$\Delta\eta_{avg,max}$	-	**24.04%**

Table 4.9: Mode shape 2, Dahl method results

As can be seen from the table summarising the results, Table 4.9, configuration 4 is the one that provides, as in the analysis using the '-3dB Method', the greatest increase in damping, although configuration 8 returns values not far different.

Chapter 5

Conclusions

The aim of this research project was to evaluate the variation of the damping factor of a non-linear system in which friction dampers were introduced to dissipate energy and reduce the vibrations transferred to the structure. A well-performed data analysis must be based on strong assumptions under well-controlled experimental conditions. It must therefore be taken into account that the experiments carried out to estimate the mass and modal stiffness were performed on the beam at the end of its life. Due to the phenomenon of fatigue damage, the beam exhibits a crack half the size of its thickness. This has certainly caused a decrease in the stiffness of the structure and this is demonstrated by the fact that the resonance peak of configuration 1 has decreased from 12.78Hz (experiment with the uncracked beam) to 11.12Hz for the first mode shape and from 71.35Hz to 69.25Hz for the second mode shape. For these reasons, the calculation of the damping factor using the Dahl method was calculated as the average of that obtained by varying the modal stiffness over a wide range of values. Another result that is considered weak is the large discrepancy between the resonance frequency value obtained between experiments and simulation with the mass at the free end; this difference may be due to a difference in the shape of the simulated mass which, due to inertia, modifies the response of the beam. One solution to attempt to obtain more accurate results than the experimental ones may therefore be to simulate a notch in the beam at the wedge and decrease the size of the added mass by increasing its density.

A relevant detail is also the inappropriate use of the "-3dB Method" applied to non-linear systems, since the dissymmetry of the FRF curve causes a great underestimation of the damping factor; the difference obtained with the two methods is in fact close to 100In conclusion, given that the system responded consistently to the modifications made, it would be interesting to extend this study to a real industrial application so that the real structural effect of the solutions found can be assessed more appropriately.

Bibliography

[1] Hamid Ahmadian and Hassan Jalali. Generic element formulation for modelling bolted lap joints. *Mechanical Systems and Signal Processing*, 21(5):2318–2334, 2007.

[2] Romain Crambuer. *Contribution à l'identification de l'amortissement: approches expérimentales et numériques.* PhD thesis, École normale supérieure de Cachan-ENS Cachan, 2013.

[3] Rod Cross. The rise and fall of spinning tops. *American Journal of Physics*, 81(4):280–289, 2013.

[4] CM Gehb, S Atamturktur, R Platz, and T Melz. Bayesian inference based parameter calibration of the lugre-friction model. *Experimental Techniques*, 44(3):369–382, 2020.

[5] Marco Rosatello. *Contribution to the study of damping in bolted structures.* PhD thesis, Université Paris-Saclay (ComUE), 2019.

[6] Peter Torvik. On estimating system damping from frequency response bandwidths. *Journal of Sound and Vibration - J SOUND VIB*, 330:6088–6097, 12 2011.